HHS Public Access

Author manuscript

Small. Author manuscript; available in PMC 2023 September 01.

Published in final edited form as:

Small. 2022 September ; 18(36): e2203003. doi:10.1002/smll.202203003.

Development of Biodegradable Osteopromotive Citrate-based Bone Putty

Xinyu Tan[a,b,c,#], **Ethan Gerhard**[b,#], **Yuqi Wang**[b,#], **Richard T. Tran**[b], **Hui Xu**[b], **Su Yan**[b], **Elias B. Rizk**[d], **April D. Armstrong**[e], **Yuxiao Zhou**[f], **Jing Du**[f], **Xiaochun Bai**[a,c,*], **Jian Yang**[b,*]

[a]Department of Cell Biology, School of Basic Medical Sciences, Southern Medical University, Guangzhou, Guangdong Province, 510515, China

[b]Department of Biomedical Engineering, Materials Research Institute, The Huck Institutes of the Life Sciences, The Pennsylvania State University, University Park, PA 16802, USA

[c]Academy of Orthopedics, Provincial Key Laboratory of Bone and Joint Degenerative Diseases, The Third Affiliated Hospital of Southern Medical University, Guangzhou, Guangdong Province, 510280, China

[d]Department of Neurosurgery, College of Medicine, The Pennsylvania State University, Hershey, PA 17033, USA

[e]Department of Orthopaedics and Rehabilitation, College of Medicine, The Pennsylvania State University, Hershey, PA 17033, USA

[f]Department of Mechanical Engineering, The Pennsylvania State University, University Park, PA 16802, USA

Abstract

The burden of bone fractures demands development of effective biomaterial solutions, while additional acute events such as noncompressible bleeding further motivate the search for multi-functional implants to avoid complications such as osseous hemorrhage, infection, and non-union. Bone wax has been widely used in orthopedic bleeding control due to simplicity of use and conformation to irregular defects; however, its non-degradability results in impaired bone healing, significant risk of infection, and significant inflammatory responses. Herein, we design a class of intrinsically fluorescent and osteopromotive citrate-based polymer/ hydroxyapatite (HA) composites (BPLP-Ser/HA) as a highly malleable press-fit putty. BPLP-Ser/HA putty displays mechanics replicating early non-mineralized bone tissues (initial moduli from ~2 – 500 kPa), hydration induced strengthening of mechanical properties in physiological conditions, tunable degradation rates (over 2 months), low swelling ratios (<10%), clotting and hemostatic sealing

*Corresponding authors: Dr. Jian Yang, jxy30@psu.edu; Dr. Xiaochun Bai, baixc15@smu.edu.cn.
#These authors contributed equally.

Declaration of Competing Interest

Dr. Jian Yang and The Pennsylvania State University have a financial interest in Acuitive Technologies, Inc. and Aleo BME, Inc. These interests have been reviewed by the University's Institutional and Individual Conflict of Interest Committees and are currently being managed by the University.

Supporting Information

Supporting Information is available from the Wiley Online Library or from the author.

potential (resistant to blood pressure for >24hrs) and significant adhesion to bone (~350–550 kPa). Key bioactive properties of citrate are further leveraged into antimicrobial (~100% and 55% inhibition of *S. aureus* and *E. coli*) and osteopromotive properties. Lastly, BPLP-Ser/HA putty demonstrates *in vivo* regeneration in a critical sized rat calvaria model equivalent to gold standard autograft. BPLP-Ser/HA putty represents a simple, off-the-shelf solution to the combined challenges of acute wound management and subsequent bone regeneration.

Graphical Abstract

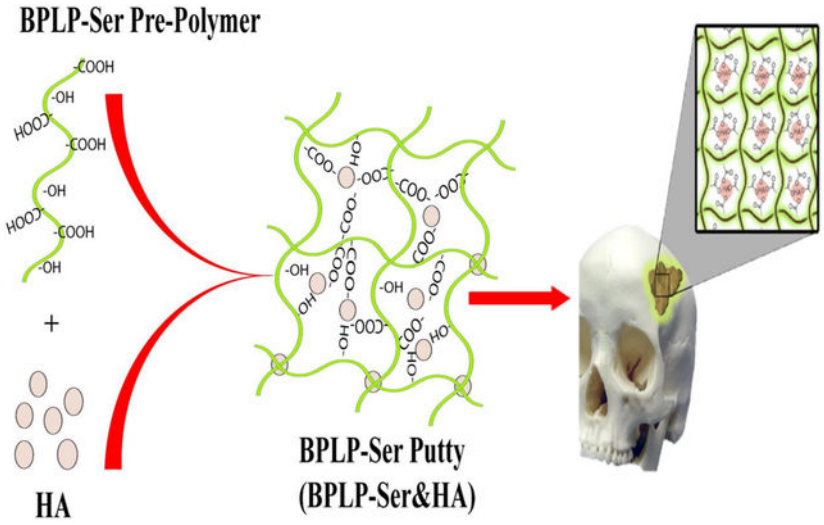

The critical chemical and bioactive properties of citric acid are leveraged into a biodegradable photoluminescent polymer/hydroxyapatite (BPLP-Ser/HA) bone putty as an off-the-shelf replacement for clinically utilized bone waxes. Obtained putty materials combine mechanical stability in physiological conditions, blood vessel sealing, and adhesion with hemostatic, antimicrobial, and osteopromotive properties, culminating in cranial bone regeneration equivalent to autograft.

Keywords

Citric Acid; Bone Wax; Bone Putty; Metabonegenesis; Orthopedic Biomaterials

1. Introduction

Bone fracture is a major public health concern globally. A systematic analysis from the Global Burden of Disease Study (GBD) revealed that there were 178 million new fractures and 455 million prevalent cases of acute or long-term symptoms of a fracture in 2019, an increase of 33.4% and 70.1% since 1990, respectively. Traumatic bone fractures and surgical bone incisions in orthopedic surgeries often result in difficult-to-control osseous hemorrhage.[1, 2] Bone wax, a waxy and hydrophobic material mainly consisting of beeswax and softening agents such as Vaseline or a mixture of paraffin wax and isopropyl palmitate, can be easily applied to the bone fracture for bleeding control in orthopedic surgeries and many other procedures such as thoracic and neurological surgeries due to its

ease of operation, satisfactory adhesion to bone, malleability and cost-effectiveness.[3, 4] However, the obvious limitations and complications of bone wax counteracting its benefits for hemostasis and orthopedic applications include: 1) markedly impaired bone healing; 2) significant risk of infection; 3) inconsistent hemostatic efficacy; and 4) significant foreign body reactions.[5–7] Therefore, current bone wax products should be restricted in surgical sites where bone fusion is desirable and can never be used in contaminated wounds. Unfortunately, despite these known limitations, beeswax-based bone wax products remain the primary choice even more than 120 years after their inception.

There have been attempts in developing bioabsorbable bone wax to address the limitations and drawbacks of beeswax-based formulations. Claimed as an “absorbable bone wax”, a Pluronic (PPG-PEG-PPG copolymer)-based bone wax substitute, Ostene was launched in 2006. Ostene can be manually softened and stick to bleeding bone as a tamponade; however, it dissolves rapidly in 1–2 days. Although the rapid dissolution and absorption of Ostene may vacate the space for bone healing to occur, Ostene itself inherently lacks osteopromotive properties (osteoconductivity and/or osteoinductivity) to help bone healing, which greatly limits its use in bones with relatively large fractures and defects. Additionally, Pluronic itself is not considered “degradable”. Thus, its *in vivo* clearance remains a concern. In the past decade, bone wax has evolved into bone paste/putty to meet the demands for improved hemostasis and osteogenesis. Alginate, cellulose, or chitosan have been blended with ceramics such as tricalcium silicate cement, bioglass, or hydroxyapatite (HA) to develop bone putty.[8–13] These bone-wax substitutes exhibit low cytotoxicity, biodegradability, and/or hemostatic functions and can also be used to deliver antibiotics, bone morphogenic proteins and cytokines to overcome the potential risk of infection and improve bone healing.[12, 14, 15] Bone glues, including commercial poly (methyl methacrylate) (PMMA), self-curing bone-wax substitute (consisting of tricalcium silicate, 58S bioglass, chitosan, carboxymethyl cellulose with KH_2PO_4 setting solution), and calcium phosphate cements (CPCs) were also used to enable hemostasis and bone healing. However, these formulations are limited by their slow degradation, necessary manual preparation steps, poor mechanical properties, insufficient fixation, moisture sensitivity, and/or inhibition of bone regeneration.[16–18] Ideal bone wax or bone putty should be: 1) ready-to-use (no preparation steps); 2) easily press-fit but sufficiently strong (comparable to cancellous bone); 3) strongly adhesive to bone; 4) hemostatic; 5) osteopromotive; 6) anti-microbial; and 7) biodegradable and bioabsorbable. However, none of the existing bone waxes or bone putties can meet all the above requirements in a single formulation.

Citrate-based biomaterials have received significant attention in recent years. Citric acid not only participates in degradable bond formation in polymers,[19] but also enhances hemocompatibility,[20] balances the hydrophilicity/hydrophobicity of polymers,[19] confers antimicrobial properties,[21] and provides additional binding sites for bioconjugation.[22] Citrate-based biodegradable polymers developed include strong yet elastic crosslinked urethane-doped polyesters (CUPE) and clickable Poly (octamethylene-citrate) (POC)-based elastomers (POC-click) for vascular and bone tissue engineering,[23–26] poly(alkylene maleate citrate) (PAMC) for injectable-based tissue engineering and endoscopic surgery, [27–30] biodegradable photoluminescent polymers (BPLP) for tissue engineering and fluorescent imaging,[31–34] and injectable citrate-based mussel-inspired bioadhesives

(iCMBA) for sutureless wound closure.[35, 36] All citrate-based biodegradable polymers investigated including POC, PAMC, BPLP, and CUPE showed considerable antimicrobial properties against Gram-negative *E. coli* and Gram-positive *S. aureus*.[37] Interestingly, the –COOH rich citrate-presenting elastomers were able to composite up to 65wt% hydroxyapatite (HA) in polymer/HA composites due to the chelation of citrate with calcium-containing particles, simulating the inorganic composition of natural bone, in contrast to traditional degradable polymers such as polylactide (PLA), which could only composite up to 25–30wt% of HA to avoid brittleness of the composites.

One of these citrate polymers, poly(octamethylene citrate) (POC),[38] has recently joined a handful of biodegradable synthetic polymers that have been developed into Food and Drug Administration (FDA)-approved/cleared medical devices. A series of POC-based bone screws and suture anchors such as Citrelock™, Citrefix™, and Citrespline™ for various orthopedic indications including knee, foot and ankle, shoulder, elbow, and wrist applications have recently received US FDA 510K clearance and are currently being distributed for the sports injury market. The regulatory success of POC-based medical devices has spurred significant interest in further developing POC into various medical devices. We have also demonstrated by incorporating amino acids during the synthesis of POC, the resultant BPLPs exhibit tunable fluorescent properties that enable imaging and sensing applications.[39, 40] More interestingly, citrate has been identified as an osteopromotive factor to mediate the metabolism and osteogenic differentiation of human mesenchymal stem cells (hMSCs) for improved bone regeneration through metabonegenic regulation.[41, 42]

To address the limitations of the current bone wax/putty, herein, a new generation of biodegradable citrate-based osteopromotive bone putty was developed by compositing a BPLP polymer synthesized by reacting citric acid (CA), 1,8-octanediol (OD), and L-Serine (Ser) with HA, referred to as BPLP-Ser/HA putty. BPLP-Ser/HA is malleable and can press-fit into irregular defects easily with comparable handling properties to bone wax. BPLP-Ser/HA was characterized via its compression strength, adhesion strength, sealing capability, swelling, hemostatic effects, pH change, and mass loss. BPLP-Ser/HA was cultured against mouse fibroblast cells (L929) to evaluate its cytocompatibility *in vitro*. Finally, a cranial bone defect rat model was used to evaluate the osteopromotive effects of BPLP-Ser/HA *in vivo* with a commercial bone wax as control.[43]

2. Results and Discussion

2.1 Intrinsically biomimetic and multifunctional BPLP-Ser/HA putty is prepared through a cost-effective one-step synthesis

Motivated by the complex hierarchical structure of bone, consisting of 60–65wt% hydroxyapatite (HA) intimately associated with an organic collagen and proteinaceous matrix, significant effort has been expended developing effective inorganic/organic composites to potentiate bone regeneration. While organic biomaterials including gelatin,[44, 45] chitosan,[46] hyaluronic acid, collagen,[47] and alginate as well as synthetic polymers such as poly(lactic acid) (PLA), poly(glycolic acid)(PGA), poly(propylene fumarate) (PPF), and poly(caprolactone) (PCL) have been extensively studied, successful

incorporation of biomimetic levels of ceramic has remained elusive, with significant instances of phase separation, brittleness and mechanical failure, and poor in vivo integration and regeneration.[48–53] Modification strategies to one or both phases, such as conjugation of ceramic binding groups to polymer chains or surface modification of ceramics with lactic acid oligomers,[54] isocyanates,[55] poly(amino acids), catechols,[53, 56] or silanes have resulted in enhanced physical properties; however, such processes are inherently limited due to the low reactivity of ceramic surface groups and increase both cost and complexity, motivating the search for composite systems with inherent biomimetic structures.[53, 57]

Citrate has emerged as a critical structural component of native bone, comprising 5% by weight and covering 1/6 of the inorganic bone surface, strongly associating with both the fibrous collagen organic phase and amorphous calcium phosphate (ACP) inorganic phase during bone formation, decreasing surface binding energy between the two phases and facilitating intra- and interfibrillar mineralization.[58–60] Further, binding of citrate to specific surfaces of HA as it undergoes crystallization from early amorphous phases serves to regulate crystal size/shape to the preferred nanocrystal morphology, preventing bulk crystal fusion and brittle mechanics.[60–63] Inspired by the dual phase bridging roles of *in vivo* soluble citrate, we theorized that polymers directly incorporating citrate could intrinsically recapitulate the strong organic/inorganic phase binding in a biomaterial platform.

BPLP-Ser prepolymer was duly synthesized (Figure 1a) via a simple, cost-effective, catalyst-free polycondensation reaction between: (1) a tetrafunctional citrate moiety enabling covalent crosslinking and ceramic chelation; (2) the naturally occurring amino acid L-Serine, enabling formation of a previously described dioxo-pyridine ring (DPR) fluorophore with high quantum yield, excellent photostability, and tunable fluorescence emission (up to 725nm),[64] and (3) difunctional 1,8-octanediol as an alkyl chain moiety, as a viscous low molecular weight oligomer. Utilizing the calcium chelating potential of the abundant free carboxyl and hydroxyl groups in BPLP-Ser oligomers, we next directly mixed their ethanolic solutions with HA to obtain BPLP-Ser/HA composites, maintaining excellent homogeneity, pliability and putty-like consistency after solvent evaporation even when HA concentration reached 65wt% (Figure 1b). Scanning electron microscopy (SEM) and EDS analysis (Supplementary Figures S1 and S2) confirmed successful integration of the ceramic phase, displaying relatively smoother and more continuous surfaces compared to commercial bone wax, well distributed HA particles uniformly incorporated within the bulk material and uniform calcium and phosphate distributions. Figure 1b further demonstrated that BPLP-Ser/HA putty is malleable and can be molded into complex structures via press-fit into various molds. BPLP-Ser/HA displayed the strong band-shifting fluorescence (330 – 725nm) (Figure 1d) inherent to the excitation-dependent DPR moiety and strong, visible green emission (580nm) (Figure 1c). Thus, we successfully leveraged citrate's unique chemistry into a branched, highly carboxylated mimic of the collagenous bone template, enabling intrinsic organic/inorganic binding and homogenization, replicating the phase composition and interaction of native bone, as a malleable press-fit putty. Further, reaction of citrate with L-Serine results in inherent material fluorescence sans utilization of toxic dyes or quantum dots, beneficial in assessing material residuals or material degradation through fluorescence imaging *in vivo* or during histological analyses. Critically

for clinical use, BPLP-Ser/HA represents a stable, off-the-shelf material capable of instant use without the need for complex mixing, toxic crosslinking agents, defined working times, or hazardous reaction conditions (free radicals, oxidizers, exothermia) that define commonly used injectable/moldable products including calcium phosphate cements (CPCs), hydrogels, and poly(methyl methacrylates) (PMMAs).

2.2 BPLP-Ser/HA putty displays mechanics comparable to early non-mineralized bone and mechanical stability in hydrated conditions

Bone's primary role as a highly mineralized support structure has seen traditional implants designed to replicate the high mechanics of the mature tissue (compressive stress ~100 – 230 MPa, modulus ~7 – 30 GPa).[65] Indeed, canonically, putty-like citrate-based polymer/HA composites have been crosslinked under prolonged and harsh thermal conditions to achieve similar values; however, such processing precludes their use in irregular defects.[53, 65] Contrary to its final properties, the initial stages of osteogenesis consist of cell mediated reorganization and mineralization of a cartilage intermediate or mesenchyme in endochondral ossification and intramembranous ossification, respectively, moving through fibrous and cartilaginous soft tissues to woven and lamellar mature bone.[66] Challenging traditional implant ideology, recent research has suggested that softer implants are better capable of replicating the dynamic properties of healing bone, optimizing the transfer of mechanical properties to cells and initiating a cascade of mechanosensitive signals necessary for endogenous healing.[67] We therefore theorized that the hitherto underutilized putty-like intermediate stage of BPLP-Ser/HA could not only enable the desired press-fit application, but attain mechanical properties comparable to the earliest stages of bone.

Accordingly, the compressive mechanical properties of BPLP-Ser/HA putties were assessed. Compressive strength and initial modulus of putties increased proportional to HA content (Figure 2). Incorporation of 55wt% HA (409.51±30.25 kPa) significantly improved the compressive strength as compared to the putties with 40wt% (1.95±0.69 kPa), 45wt% (56.11±4.97 kPa), and 50wt% HA (116.67±7.77 kPa) in dry conditions (Figure 2a), reinforcing the role of HA both as macro-crosslinker via the multiple strong binding interactions with the BPLP-Ser polymer and as a high strength ceramic material. Similarly, the initial modulus also significantly increased as the concentration of HA was increased (1.08 ± 0.36, 67.1 ± 4.69, 99.49 ± 18.91, and 427.22 ± 84.98 kPa for 40, 45, 50, and 55wt% HA) (Figure 2b). Interestingly, in contrast to most biomaterials, the compressive strength of the putties increased under wet conditions, which is beneficial for *in vivo* application. The compressive strength for the putty with 45%, 50%, and 55wt% HA significantly increased to 91.22 ± 7.33, 285.69 ± 30.35, and 764.80 ± 60.61 kPa, respectively, following submersion in phosphate buffered saline (PBS) at 37°C for 24 hours. In contrast, putty containing 40wt% HA lost mechanical stability, elucidating the importance of sufficient inorganic content to material cohesion and highlighting the physio- mechanical advantages of the BPLP-Ser/HA putty vs. pure BPLP-Ser *in vivo*. While the same trend was observed in initial modulus, the differences between the dry and wet mechanics were not significant (Figure 2b). The strength of conventional bone wax was significantly lower than the BPLP-Ser/HA putty with 50% and 55% HA and similar to the 45% HA formulation under both dry and wet conditions; however, the initial modulus was much greater (49.98 ± 5.57 MPa and 59.19

± 5.70 MPa in dry and wet conditions, respectively). Additionally, we also observed an increase in initial modulus under wet conditions compared to the dry condition, consistent with the putty. While the underlying mechanism of the increased wet mechanical properties of BPLP-Ser/HA putty is not entirely clear, we reasoned that: (1) the absorption of PBS by the putty helps ionize carboxyl groups in the BPLP-Ser polymers which can better chelate with calcium-containing HA particles, and (2) defined hydrophobic (diol) and hydrophilic (citrate) regions within BPLP-Ser polymers preferentially reorient in a bulk non-solvent (in this case aqueous PBS), increasing material density and thus mechanics, concurrent with results observed in diverse materials including poly(HEMA) hydrogels and poly(ethylene glycol) (PEG)-poly(lactide-co-glycolide) (PLGA) block polymers.[68] Further, previous formulations of thermally crosslinked citrate-based materials incorporating long chain hydrophobic diols revealed formation of distinct hydrophobic association regions, lending shape memory properties and increased mechanics under extended wet conditions.[69] To further elucidate the relative contribution of the two above effects, mechanics were next tested following hydration in deionized (DI) water, revealing a further increase in strength (126.64 ± 10.45, 147.04 ± 13.10, 338.19 ± 20.87, and 1,134.29 ± 105.02 kPa for Bone Wax, and BPLP-Ser putty with 45, 50 , and 55%HA, respectively) as well as initial modulus (95.19 ± 10.35, 375.86 ± 30.92, and 1,000.73 ± 87.62 kPa for putty with 45, 50, and 55%HA (modulus of Bone Wax in contrast was similar to the PBS value, reaching 50.29 ± 8.12 MPa)) (Figure 2c and d). In light of the above results and given the relative polymer chain freedom in BPLP-Ser/HA putties crosslinked by chelation only, it can be posited that in response to the non-solvents PBS and DI water, diol regions are capable of such reorientation (such reorientation of long hydrophobic chains could also explain the increased wet mechanics of commercial bone wax, which lacks both significant ionizable groups and HA) and that this effect is dominant in comparison to ionization of carboxylates (additionally, phosphate anions present in PBS may interfere with carboxylate-HA interactions, counteracting this benefit). Finally, incubation in whole blood resulted in similar or increased strengths (156.13 ± 13.07, 127.91 ± 22.40, 442.22 ± 19.23, and 1,000.73 ± 87.62 kPa) and moduli (46.77 ± 6.51 MPa and 156.70 ± 24.17, 586.32 ± 90.56, and 1, 567.42 ± 292.50 kPa) compared to DI water (Figure 2c and d). Tellingly, a well-defined layer of coagulated blood was observed on the surface of all BPLP-Ser putty formulations that was absent from Bone Wax, indicating significant interactions between the putty surface and blood cells/proteins. Given the large calcium content inherent to BPLP composites, it can be inferred that calcium cations within the bulk material or released into the local environment are capable of mediating clotting and further that the resulting crosslinked protein network is capable of interacting with and mechanically reinforcing the material. Strong interfacial binding between the inorganic BPLP-Ser polymer phase and HA inorganic phase, with HA particles acting as macro-crosslinker and calcium reservoir, thus resulted in a material with tunable mechanics achieving both comparable handleability to bone wax, critical to its application, and similar mechanics to materials promoting osteogenic differentiation (modulus ~15 kPa – 30 MPa), further reinforcing BPLP-Ser/HA as a biomimetic platform, with significant hydration induced strengthening in physiological conditions, beneficial to sealing and reinforcement of fractured and bleeding bone *in vivo*.[70, 71]

2.3 BPLP-Ser/HA putty achieves tunable degradation rates and swelling ratios while maintaining material stability

Proper material degradation rate is critical to ensure effective bone regeneration, with rapid degradation leading to inability to properly stabilize defects and allow time for new tissue formation, while extended degradation conversely prevents tissue ingrowth, delaying proper defect healing. Traditional thermally cross-linked citrate-based composites display long degradation times (10 to 20wt% in 1 year);[53] however, we posited that utilizing BPLP-Ser/HA putty containing only ionic and chelation bonds, an intermediate degradation rate (months) could be achieved (as opposed to pure BPLP oligomers with rapid degradation rates of ~2 weeks).[72] Verification of degradation mass loss was thus performed (Figure 3a). Interestingly, HA concentration did not significantly influence the degradation rate of the putty within the first 4 weeks. It wasn't until week 6 that BPLP-Ser putty synthesized with the least amount of HA (40 wt%) showed a significantly higher mass loss of 75.58 ± 4.17%, whereas all other formulations had approximately half their mass remaining; however, at 8 weeks BPLP-Ser/40% HA was completely degraded while the average mass loss of BPLP-Ser/45% HA was 97.37 ± 2.10%. In contrast, BPLP-Ser/50% HA and BPLP-Ser/55% HA exhibited an average of nearly 60% mass loss at 8 weeks, again reinforcing the role of HA as composite crosslinker (as well as a more hydrophobic and stable component), with increased HA leading to longer degradation times. Concomitant evaluation of degradation pH revealed a sharp decrease to acidic values (<7) within the first 2 weeks, gradually recovering by the 3rd week and remaining stable thereafter (Figure 3b). Similar to mass loss, no significant difference was observed between HA concentrations at each time point. While such initial pH drops may be of concern *in vitro*, it should be considered that: (1) the initial stages of bone remodelling post-fracture involve the activation of large populations of osteoclasts which subsequently excrete acid locally to initiate dissolution of the ceramic bone phase, liberate necessary constituent minerals, and activate growth factors such as transforming growth factor beta (TGF-b), thus a locally temporary acidic microenvironment is a necessary component of healing;[66, 73] (2) rates of clearance of degradation products *in vivo* are enhanced due to active uptake by cells as well as diffusion into local vasculature, and (3) the primary mediator of pH drop in BPLP-Ser/HA materials, citrate, is a necessary metabolite whose cellular uptake is upregulated in differentiating osteoblasts, leading to its rapid local uptake.[42] Therefore, rather than a potential concern, release of acidic citrate could function to better mimic local conditions and cellular need *in vivo*.

The high swelling ratios of many injectable polymeric systems (such as hydrogels which can swell 100% or even 1000%),[74] potentially causing post-operative pain, pressure induced damage to peri-defect tissues (particularly in the brain and spinal regions), and potential implant dislodgement, lead to reduced patient satisfaction and impaired healing. Swelling ratios of BPLP-Ser/HA putties in PBS were thus compared along with commercial bone wax (Figure 3c). Significantly different swelling ratios of 5.55 ± 0.12, 4.98 ± 0.06, and 4.05 ±0.09% were obtained for BPLP-Ser/45% HA, BPLP-Ser/50% HA, and BPLP-Ser/55% HA, respectively, while bone wax displayed a swelling ratio of 1.25 ± 0.03%, significantly lower than all BPLP-Ser/HA formulations, expected due to the higher hydrophobicity of the purely alkyl chain wax relative to BPLP-Ser/HA. Nonetheless, BPLP-Ser/HA composites

demonstrated an advantageous, low swelling character. In line with their minimal swelling ratios and extended degradation times, BPLP-Ser/50% HA composites demonstrated significant bulk stability *in vitro*, maintaining their initial dimensions sans noticable swelling or significant fragmentation even after 12 weeks, suggesting that residual organic/inorganic crosslinks maintain a stable network even after significant bulk mass loss (>60%) (Figure 3d). Stability assesment also served to highlight the significant difference in material density between BPLP-Ser/HA and bone wax (Figure 3e). BPLP-Ser/50% HA displayed a density of (1.69 g/cm^3), comparable to explanted rat calverial bone (1.61 g/cm^3) and matching literature values for human bone (1.62 – 1.92 g/cm^3),[75] further confirming the biomimetic nature of BPLP-Ser/HA. In contrast, bone wax had a significantly lower density (0.92 g/cm^3), enabling its bouyancy in PBS (leading to increased likelyhood of extravasation of small particles through local vasculature) (Figure 3d). In sum, physical characterization of BPLP-Ser/HA putty revealed significantly tunable properties through control of material composition, achieving degradation rates intermediate between the ultra-rapid degradation of current biodegradable bone waxes such as Ostene (1–2 days) and the lengthy degradation or non-degradability of CPC cements and PMMAs, respectively, enabling functionality both as acute fracture sealing agents and support for tissue regeneration. Further, effective polymer/HA interactions and high HA loading capability resulted in low swelling ratios, effective material stability and increased material density, reducing the likelyhood of material failure, dislodgement, and extravasation compared to non-degradable bone waxes (an additional benefit of degradabilty being eventual dissolution of dislodged particles in vivo).

2.4 BPLP-Ser/HA putty achieves hemostatic and adhesive properties

Rapid and effective bleeding control is necessary in multiple orthopedic surgeries as well as a number of other surgeries requiring bone incision. Commercial bone wax enables clot formation via infiltration and physical occlusion of blood vessels, known as the tamponade effect.[76, 77] We reasoned that BPLP-Ser/HA, by vitrue of its malleable initial character combined with excellent stability and hydration induced strengthening capabilities, would perform capably as a tamponade material and further that calcium release would actively enhance blood clotting, as discussed in Section 2.2. Hemolysis was first assessed to determine the effect of materials on erythrocytes, revealing significantly higher lysis (23.64 ± 0.62, 25.05 ± 0.77, and 24.71 ± 2.23 % for BPLP-Ser with 45, 50, and 55%) in the presence of putty vs. Bone Wax (1.16 ± 0.15%) (Figure 4a), likely due to local pH drop and release of calcium cations, both known mediatiors of erythrocyte cell membrane disruption (the latter particularly attested to in response to silver cations);[78, 79] however, it should be considered both that these values are within the range of other hemostatic materials and that BPLP-Ser putty is not designed for prolonged blood contact (indeed being sealed off from active blood flow by clotting), reducing the effect of hemolysis beyond the acute stage.[80–82] Whole blood clotting time was next assessed, demonstrating a significant decrease in clotting time for all BPLP-Ser putty formulations compared to control and Bone Wax (12.33 ± 0.26, 11.75 ± 0.69, and 11.33 ± 0.41 minutes for 45, 50, and 55% HA vs 14.92 ± 0.38 and 14.75 ± 0.52 minutes for control and Bone Wax) (Figure 4b), confirming the capability of putty to pomote clotting, acting as an active hemostat in comparison to Bone Wax and demonstrating reduction in clotting time (~17, 21, and 24%) comparable to

other solid hemostats.[81] Sealing potential of BPLP-Ser/HA putties and commercial bone wax was evaluated using the previously described liquid sealing test with modifications (Figure 4c).[83] Briefly, a gravity induced pressure head equivalent to physiological blood pressure in amputated medullary cavities (140mmHg)[77] was established by filling a 2 meter vertical polypropylene tube sited within a 37°C incubator with blue dye. A defined amount of sealant material was then compressed by hand within the bottom tube opening, forming the initial plug seal. The lower end of the tube was finally placed within a beaker containing clear PBS, simulating wet physiological conditions and enabling easy leakage detection. BPLP-Ser/45% HA failed most rapidly (<20 minutes), due to its relatively weak mechanics, while commercial Bone Wax occluded flow for 2 hours (Figure 4d) followed by failure. In contrast BPLP-Ser/50% HA and BPLP-Ser/55% HA withstood physiological pressure for 24 hours, significantly longer than bone wax and the typical in vivo clotting time (8 – 15 minutes),[84] which could be beneficial in cases of compromised clotting or clot dislodgement during or post-surgery. In vitro sealing thus confirmed the favorable performance of BPLP-Ser/HA as tamponade material while highlighting the importance of a high HA loading.

Effective blood vessel occlusion in the bone environment additionally requires the ability to successfully adhere to and infiltrate the porous native bone surface. In light of the demonstrated ability of BPLP-Ser to bind HA, the chemical structure of BPLP-Ser, including free carboxyl and hydroxyl groups, is expected to bind strongly with the bone tissues through hydrogen bonds, hydrophobic interactions, and ionic interactions, in contrast to commercial Bone Wax and PMMAs, which depend predominantly on mechanical interlock rather than active binding moieties.[85, 86] As shown in Figure 4e, adhesion strengths to trabecular bone of putty formulations were higher than Bone Wax (399.74 ± 43.49, 366.27 ± 42.99, and 557.35 ± 17.04 kPa for 45, 50, and 55%HA vs. 187.57 ± 4.57 kPa for Bone Wax) as well as meeting or exceeding values obtained for calcium phosphate cements, PMMA, and hydrogel based sealants.[17] Enhanced adhesion of BPLP-Ser/50% HA versus bone wax was further demonstrated via a femoral condyle reattachment model utilizing chicken tissue, in which BPLP-Ser/50% HA was able to bond strongly enough to support the weight of the complete chicken leg while bone wax failed (Figure 4f). BPLP-Ser/50% HA also demonstrated the ability to seal the femoral intramedullary cavity of wet chicken tissue (amputation model) (Figure S3) comparable to bone wax. BPLP-Ser/HA thus demonstrated potential in promoting clotting, resisting blood pressure and enabling wet tissue adhesion.

2.5 BPLP-Ser/HA is an intrinsically antimicrobial biomaterial

Surgical and implant associated infection is a common occurrence, leading to inflammation, pain, impaired healing and tissue necrosis, necessitating development of effective antimicrobial biomaterials. While various modification strategies have been adopted to confer antimicrobial properties to polymers, including the introduction of quaternary ammonium salts and antimicrobial peptides into the polymers, incorporation of antimicrobial ions such as copper, silver, and zinc, and encapsulation or conjugation of antimicrobial drugs such as gentamycin are common, materials demonstrating inherent antimicrobial potential offer attractive alternatives in terms of lower material complexity and

cost.[87–89] Soluble citrate functions as a potent antimicrobial agent, utilized in multiple germicidal formulations, dental rinses, and agricultural bactericides.[90] Citrate is thought to inhibit bacteria via lowering of intercellular pH, inducing DNA, protein and membrane damage as well as inhibiting nicotinamide adenine dinucleotide (NADH) oxidation, leading to cell death, as well as through direct, disruptive binding to cell membranes and chelation of calcium and magnesium cations required for cellular function and growth.[37, 90] Accordingly, citrate-based materials have uniformly displayed antimicrobial function dependent on relative citrate content and degree of crosslinking.[37] It was therefore expected that BPLP-Ser/HA putties, being minimally crosslinked and mediating a pronounced acute pH drop in vitro as described in Section 2.3, would be excellent candidates as intrinsically antimicrobial composites. Accordingly, BPLP-Ser/HA putty was tested against *Staphylococcus aureus* (S. aureus) and *Escherichia coli* (E. coli) with an initial bacterial concentration of 1×10^6 CFU/ml as representative Gram-positive and Gram-negative species with bone wax serving as control. As shown in Figure 4a and 4b, optical densities of *E.coli* and *S.au* treated with BPLP-Ser/45% HA, 50% HA, and 55% HA were significantly decreased compared to both positive and Bone Wax controls following 24 hours of incubation, while no siginificant difference was observed between putty formulations, illustrating the minimal impact of HA content. All BPLP-Ser/HA formulations exhibited better performance against *S.au* compared to *E.coli*, with the optical densities of the former diminished to a level similar to pure media. BPLP-Ser/HA and bone wax displayed inhibition ratios between 50–55% and 25% against *E. coli*, respectively (Figure 4c), while the inhibition ratios of BPLP-Ser/HA against *S.au* were nearly 100% (Figure 4d). In contrast, Bone Wax displayed negative performance. BPLP-Ser/HA putties represent a novel class of antimicrobials via effective citrate release, in stark contrast to commercial bone waxes and many other moldable/injectable materials which require modification with or loading of distinct antimicrabial agents, facilitating effective prevention and treatment of infection.

2.6 BPLP-Ser/HA displays biocompatibility and osteopromotion

Biocompatibility of BPLP-Ser/45% HA, 50% HA, and 55% HA degradation products was assessed via CCK-8 assay against L929 cells (Figure 5a) with PLGA 75:25 as control. At the highest concentration (1x), cell viabilities of BPLP-Ser/HA formulation treated cells were significantly lower (<5%) compared to PLGA (~60%), while cell viabilities increased with decreasing degradation product concentration. At 5x dilution, cell viabilities of BPLP-Ser/45% HA and BPLP-Ser/50% HA groups increased to (~60%), whereas cell viability in the BPLP-Ser/55% HA group reached ~80%, equivalent to PLGA. Further, at 10x and 100x dilutions, cell viabilities in all groups were equivalent, displaying minimal toxicity. The effects of BPLP-Ser/45% HA, 50% HA, and 55% HA degradation products on cell proliferation were also studied, again utilizing PLGA as control (Figure 5b). Cell numbers uniformly increased from Day 1 to Day 3 and from Day 3 to Day 5, while microscopy revealed increased numbers of adherent cells displaying normal spread morphology (Figure S4). Cell viabilities of each group exposed to 10x, 50x, and 100x diluted products after 3 days were similar, corresponding to the trends in cytotoxicity, while at Day 5, cell numbers in the groups treated with 50x and 100x diluted degradation products of BPLP-Ser/HA were significantly higher than both untreated and PLGA controls. These results

suggest that degradation products of BPLP-Ser/HA putties are not significantly toxic to cells except at the highest concentration (which given the prolonged degradation period of BPLP-Ser/HA and significant *in vivo* clearance is not expected to be attained under physiological conditions) and that less concentrated products in fact promote cell proliferation, in line with previous citrate-based materials and constituent monomers.[91] Additionally, direct seeding of human mesenchymal stem cells (hMSCs) on BPLP-Ser/50%HA resulted in successful proliferation (Figure S5). While cell growth was initially limited (111.76 ± 1.87% at Day 3), likely due to pH change and leaching of soluble products from the bulk material, cell numbers more than doubled by Day 7 (247.27 ± 7.02%) and increased more than 10-fold by Day 14 (1,107.35 ± 48.25%) when compared to Day 1, indicating that while BPLP-Ser/HA may present a challenging cellular environment in the acute phase, it is capable of supporting significant cell growth.

Osteogenic capability is a critical benchmark in the transition from inert to bioactive bone implants. Citrate, long recognized as a critical structural component of bone, has more recently been implicated as a critical bioactive factor in osteogenesis.[92, 93] Our previous research identified citrate as a key osteopromotive factor, mediating osteogenic differentiation through uptake of soluble citrate by the solute carrier family 13, member 5 (SLC13a5) channel and subsequent regulation of metabolic pathways centered on the canonical tricarboxylic acid (TCA) cycle, fueling the high energy demands of differentiating hMSCs and promoting downstream osteogenic processes (termed the metabonegenic effect).[41, 42] We therefore assessed the osteogenic differentiation of hMSCs in the presence of osteogenic media containing 50x and 100x diluted BPLP-Ser/HA degradation products via expression of alkaline phosphatase (ALP) and calcium deposition with pure osteogenic media (OG) as control (Figure 6c). ALP levels were similar for all groups at Day 7, while Day 14 ALP levels for BPLP-Ser/45% HA, BPLP-Ser/50% HA, and BPLP-Ser/55% HA at both 50x and 100x dilution were lower than the OG control; however, ALP levels for all BPLP-Ser/HA groups increased significantly from Day 7 to Day 14, indicating successful osteogenic differentiation. Further, hMSCs exposed to BPLP-Ser/HA uniformly displayed calcium nodule formation at Day 14 with no significant difference observed between BPLP-Ser/HA groups and OG control, indicating successful mineralization in the presence of degradation products (Figure 6d). These results support the osteopromotive effect of BPLP-Ser/HA derived citrate, in line with previous *in vitro* and *in vivo* studies.[41, 94]

2.7 BPLP-Ser/HA putty promotes cranial bone regeneration equivalent to autograft

Positive in vitro results as outlined above motivated in vivo testing of BPLP-Ser/50% HA (chosen to balance material handling, degradation, and bioactive properties) against negative (NC-) and positive (autograft) controls as well as commercial Bone Wax in a critical-sized full-thickness cranial defect rat model. Cranial defects were chosen due to their well-known reduced healing response, a function of poor blood supply and deficiency of bone marrow sources (thus representing a severe defect model), as a commonly occurring and easily accessible irregular defect well suited to press-fit materials, and as a defect in which Bone Wax is commonly utilized (particularly in cases of neural procedures).[95, 96] 8-mm cranial defects were created, resulting in significant bleeding (Figure S6c, d, and e), followed by

application of the appropriate material (preventing further bleeding in the case of BPLP-Ser/50%HA and Bone Wax (Figure S6f and Figure S7a and b) (detailed surgical procedure provided in Materials and Methods and Figures S6 and S7) and wound closure.

Rats displayed minimal discomfort and lacked overt signs of infection or chronic inflammation, with complete soft tissue and skin healing occurring normally regardless of implant. Skulls were harvested at 1 week and 4 weeks post-surgery for evaluation of bone regeneration. Micro-computed tomography (uCT) analysis revealed complete coverage of the defect area (red circle) in both the autograft and BPLP-Ser/HA groups with their respective implants, highlighting the prolonged stability of BPLP-Ser/HA putty compared to resorbable Bone Waxes (Figure 7a). Isolation of the defect area revealed similar bone ingrowth around the periphery of all groups, indicating bone regeneration was successfully initiated (Figure 7b). After 4 weeks, BPLP-Ser/HA was no longer observed within the defect, confirming its degradable nature (the relatively rapid degradation of BPLP-Ser/HA *in vivo* compared to *in vitro* (4 weeks vs. > 8 weeks) was likely mediated by active enzymatic degradation of polymers and active resorption of HA by cells), while around 1/2 of the autograft had been resorbed (a common occurrence when large, living bone segments are separated from native vasculature and nutrient networks and a severe limitation in autografting procedures). Minimal bone growth was observed in the negative control and bone wax groups compared to week 1, while bone regeneration within the bone wax group even appeared lower than the negative control, in line with previous research demonstrating inhibited tissue regeneration in the presence of such non-resorbable materials.[4] In contrast, significant bone ingrowth was seen in the autograft and BPLP-Ser/HA groups, with BPLP-Ser/HA appearing equivalent or superior. Quantitative bone volume to tissue volume (BV/TV) ratios were then extracted from uCT data (Figure 7c). No difference was observed among groups at 1 week; however, the BV/TV ratios of the autograft (21.01% ± 2.84%) and BPLP-Ser/HA (19.49% ± 2.79%) groups were higher than those of the negative control and bone wax at week 4, while no difference was observed between autograft and BPLP-Ser/HA. Indeed, BV/TV of both the negative control and bone wax groups barely increased from week 1 to week 4, in stark contrast to the more than 4-fold increase in both the autograft and BPLP-Ser/HA groups. These results support the regenerative effects of BPLP-Ser/HA (equivalent to the gold standard autograft treatment) compared to conventional bone wax. Fluorescent imaging of tissue explants (Figure 7d) demonstrated strong green fluorescence of residual BPLP-Ser/HA at week 1, while at week 4 no fluorescent signal could be observed, confirming complete material degradation within 4 weeks while supporting the application of BPLP-SER/HA toward *in vivo* monitoring of material degradation.

Transverse defect sections were stained with hematoxylin and eosin (H&E) and compared to associated transverse uCT images to further examine tissue regeneration (Figure 8). Only loose fibrous tissue (indicative of early loose, non-mineralized mesenchyme tissue inherent in intramembranous ossification) was observed in the negative control and bone wax groups at both week 1 and week 4 (Figure 8a–b, g-h) as confirmed by uCT. The presence of non-resorbable bone wax was also confirmed in the transverse uCT slices at week 1 and week 4. Autograft could be readily observed along with fibrous tissue at both 1 and 4 weeks (Figure 8c–d) while at week 4 resorption of the implant was evident along with new bone formation,

consistent with the results from Figure 7. At week 1, fibrous tissue surrounded the BPLP-Ser/HA implant; however, it did not penetrate into the defect, while at week 4 significant new bone formation was observed in addition to fibrous tissue as well as complete resorption of the implant (Figure 8e–f). The presence of macrophages was observed at week 1 in the bone wax, BPLP-Ser/HA and negative groups, indicating an acute inflammatory response (Figure 8a, e, and g); however, this was completely resolved in all groups by week 4, demonstrating that despite initial leaching of citrate from BPLP-Ser/HA materials, no significant chronic inflammation or adverse tissue response results. Additionally, at week 4, a denser fibrous tissue indicative of compact mesenchyme was observed in the BPLP-Ser and autograft groups compared to week 1 (Figure 8d and f), with large numbers of cells present, particularly adjacent to new bone (Figure 8i and j), further indicating regeneration of non-mineralized pre-bone tissue (indicating further development among the stages of intramembranous ossification: loose mesenchyme, compact mesenchyme, and formation of mineralized bone compared to the negative control and Bone Wax). At larger magnifications, osteoblasts were shown to be aligned along the surface of newly formed dense bone tissue in both the autograft and BPLP-Ser/HA groups (Figures 8i and j, respectively, green arrows), indicating active bone formation. Additionally, a large number of blood vessels were observed in both groups (black arrows), establishing critical neo-vasculature. Combined and supported by the uCT and BV/TV data, these findings confirm the regenerative potential of BPLP-Ser/HA as both superior to traditional bone wax and an equivalent alternative to autograft via the pro-osteogenic and angiogenic effects of citrate.

3. Conclusion

In summary, we have synthesized a new class of off-the-shelf, highly tunable citrate-based fluorescent putty-like materials as effective alternatives to clinically prevailing bone waxes. Leveraging the unique role of citrate as a bridge between the organic and inorganic phases of native bone, a strongly bound composite capable of homogeneously incorporating physiological levels of hydroxyapatite was obtained while maintaining soft mechanics and excellent handling. Obtained materials demonstrated hydration induced strengthening in physiological conditions, tunable degradation rates, minimal swelling, promotion of blood clotting, hemostatic sealing potential and enhanced adhesion to bone. Further, sustained citrate release enabled inherent antimicrobial and osteogenic potential. Finally, the novel reaction of L-Serine with citrate resulted in intrinsically fluorescent materials enabling ex vivo assessment of material degradation kinetics. Convergence of citrate’s material-chemical and biological advantages in vivo led to calvaria bone regeneration greater than that obtained using commercial Bone Wax and equivalent to gold standard autograft. In future, citrate-based putty is envisioned as a platform material benefitting from the significant tunability and modification potential of the citrate material family. For instance, degradation rates could be further extended via diol selection to accommodate differential tissue regeneration rates, enhanced bioactive properties could be incorporated via chemical conjugation or compositing, and fluorescence tracking could enable in vivo material monitoring. Citrate-based putty thus represents a new paradigm of intrinsically bioactive and multi-functional biomaterials toward effective clinical treatment of bone fractures and defects where the current bone wax is used.

4. Materials and Methods

4.1. Materials

Hydroxyapatite (HA) (Mw: 502.32, assay > 90% (as Ca_5 (PO_4) 3(OH)); particle size: > 75 μm (0.5%), 45–75 μm (1.4%), < 45 μm (98.1%)) was purchased from Fluka (St. Louis, MO, USA). Commercial Bone Wax (ETH-W31G) was purchased from Ethicon (Cincinnati, OH, USA). Citrated bovine whole blood was purchased from Lampire Biological Laboratories (Pipersville, PA). All remaining chemicals were purchased from Sigma-Aldrich (St. Louis, MO, USA) and used as received unless stated otherwise.

4.2 Phase purity analysis of hydroxyapatite

The phase purity of hydroxyapatite was assessed via X-Ray Diffraction (XRD) using an Empyrean II Diffractometer (Malvern Panalytical, Westborough, MA) from 0° to 80° 2 ▫ and analyzed in JADE (MDI/ICCD, Newton Square, PA) (Figure S8).

4.3 Biodegradable photoluminescent composite putty synthesis

Aliphatic biodegradable photoluminescent pre-polymers were synthesized by the copolymerization of citric acid with 1,8-octanediol and L-serine in a 1.0:1.0:0.2 molar ratio. Briefly, a mixture of citric acid, 1,8-octanediol and L-serine were added to a 100 mL three-necked round bottom flask fitted with an inlet and outlet adapter. The mixture was melted under a flow of nitrogen gas by stirring at 160°C in a silicone oil bath. The temperature of the system was subsequently lowered to 140°C and allowed to react for 2 h to create a biodegradable photoluminescent pre-polymer (pre-BPLP-Ser). To remove any of the unreacted monomers and oligomers, the pre-polymer was dissolved in 1,4-dioxane and purified by drop wise precipitation in deionized water (DI) produced from a Direct-Q5 Water Purification System (Millipore, Billerica, MA). The undissolved pre-polymer was collected and lyophilized in a Freezone 6 Freeze Dryer (Labconco, Kansas City, MO) to obtain the purified pre-BPLP.

To synthesize fluorescent bone putties, pre-BPLP-Ser was composited with HA in various weight ratios. Briefly, pre-BPLP-Ser was dissolved in ethanol to create a 50 wt% solution. Next, HA was added to the solution at a predetermined wt% to pre-BPLP-Ser and mixed in a Teflon dish pre-warmed to 80°C to aid in solvent evaporation. The resulting putty is denoted as BPLP-Ser/X HA where X represents the HA weight percentage in the putty. For example, BPLP-Ser/50% HA indicates that 50 wt% HA was chosen for putty synthesis.

4.4 Composite morphology

To assess the morphology and homogeneity of BPLP composites, disks 6 × 2 mm (diameter × height) were formed via press-fit into PDMS molds. Composites were subsequently removed, mounted for SEM imaging, and sputter coating with a 5nm iridium layer (Emitec Sputter-Coater). Samples were imaged using an Apreo S LoVac SEM (Thermo Fisher Scientific, Waltham, MA). EDS analysis was conducted using AZtec (Oxford Instruments, Abingdon, UK).

4.5 Composite Mechanics

Unconfined compression tests were performed using a 5966 series advanced electromechanical testing system with a 10kN load cell (Instron, Norwood, MA, USA). Briefly, cylindrical shaped samples 6.5 × 13 mm (diameter × height) were compressed at a rate of 1.3 mm min^{-1} to 50% strain. Values were converted to stress-strain and the initial modulus (kPa) was calculated from the initial gradient of the resulting curve (0–10% compressive strain). Wet mechanical properties were conducted as above on cylindrical samples incubated in phosphate-buffered saline (PBS) (pH 7.4), deionized (DI) water, or bovine whole blood at 37 °C under orbital shaking (200 rpm) for 24h.

4.6 Composite Swelling

The swelling percentage was measured by the mass differential after incubation of the composite network in phosphate-buffered saline (PBS) at 37 °C under orbital shaking (200 rpm). Briefly, 6 × 2 mm (diameter × thickness) disc shaped samples were weighed to find the initial mass (W_i) and suspended in PBS for 24 h. The samples were removed from the PBS, blotted dry with filter paper, and weighed (W_s). The swelling percentage was calculated using the formula from equation (1):

$$Swelling\ (\%) = (Ws - Wi)/\ Wi \times 100\% \quad (1)$$

4.7 Composite Degradation

The degradation rate of 6 × 2 mm (diameter × thickness) disk shaped samples was assessed *in vitro* using phosphate-buffered saline (PBS) (pH 7.4) at 37°C under orbital shaking (200 rpm). The PBS was changed every week to ensure that the pH did not drop below 7. Prior to weighing, samples were extensively rinsed with deionized water and lyophilized. Weight loss was calculated by comparing the initial weight (W_i) with the weight measured at 1, 2, 4, 6, and 8 weeks (W_t), as shown in equation (2).

$$Mass\ loss\ (\%) = (Wt - Wi)/\ Wi \times 100\% \quad (2)$$

pH of the degradation media was assessed at each time point using an Orion™ 4 Star Benchtop pH meter with an Orion™ 8102BN ROSS™ Combination pH Electrode (Thermo Fisher Scientific, Waltham, MA).

4.8 Composite Density

Composite Density was assessed using the density accessory for the Mettler Toledo XP504 balance (Mettler Toledo, Columbus, MN) at room temperature and with DI water as the auxiliary fluid. Briefly, 6 × 2 mm (diameter × thickness) disk shaped samples were first weighed in air to determine (W_a). Samples were then immersed in the auxiliary fluid bath to determine (W_b). Density was then calculated according to equation (3):

$$Density\ (g/cm3) = (Wa/(\ Wa - Wb))\ x\ (p0 - pL) + pL \quad (3)$$

where p_0 = the density of DI water, and p_L = the density of air (0.0012 g/cm^3).

4.9 Photoluminescent characterization

Photoluminescent properties of composites were studied using a Horiba FluoroMax-4 spectrofluorometer (Horiba Scientific, Edison, NJ). The fluorescent spectra of composites (1cm diameter × 2mm thickness) were measured using a solid-state holder (Horiba Scientific, Edison NJ) with excitation and emission slit sizes of 1.5 nm by 1.5 nm and step size of 10nm. Fluorescent images of composites were also obtained using an in vivo fluorescent imaging system (MaestroTM EX, Woburn, MA) with excitation and emission wavelengths of 370 and 580 nm, respectively.

4.10 Hemocompatibility

Hemocompatibility of bone wax and composites was assessed via a previously reported method.[80, 81, 97] Briefly, 0.125g of bone wax or BPLP-Ser composite was added to a 1.5mL microcentrifuge tube and tamped with a Teflon rod to achieve uniform surface areas (500uL of PBS and 0.1% Triton X-100 solution in DI water served as negative and positive controls, respectively. Bovine whole blood was diluted 50x with PBS and 500uL of diluted blood was added to each sample followed by incubation at 37°C with shaking (100rpms) for 1 hour. After 1 hour, 500uL of PBS was added to bone wax and BPLP-Ser composite samples to normalize concentration with the positive and negative controls. Samples were then centrifuged at 2000 rpms for 10 minutes and 200uL of supernatant was pipetted into the wells of a 96 well plate. Absorbance was read at 545nm using a plate reader (infinite M200 PRO, TECAN, Männedorf, Switzerland). Hemolysis (%) was calculated according to equation (4):

$$Hemolysis \quad (\%) = \left(\frac{As - Aneg}{Apos}\right) * 100 \tag{4}$$

where A_s = absorbance of the sample, A_{neg} = absorbance of the negative control, and A_{pos} = absorbance of the positive control.

4.11 Whole Blood Clotting Time

Blood clotting time of bone wax and composites was assessed according to a previously described method.[80, 81, 97] 0.125g of bone wax or BPLP-Ser composite was added to a 1.5mL microcentrifuge tube and tamped with a Teflon rod to achieve uniform surface areas (blank microcentrifuge tubes served as control). Citrated bovine whole blood was reactivated by mixing with 0.1M $CaCl_2$ (10% v/v) followed by mixing for 10s. 100uL of blood was then added to each sample and samples were incubated at 37°C. Clotting time was assessed via tilt testing every 30s, with formation of a non-flowable clot mass designated as the end point.

4.12 Hemostatic Sealing Test

Sealing capability of composites was assessed via a commonly utilized tube sealing method. Briefly, 2mm vertical lengths of clear polyethylene tubing were attached to the wall of a 37°C incubation room. Blue dye was then inserted via syringe attached to the top of the tube until the entire tube length was filled. Composite material was then inserted into the bottom of the tube to create a seal, after which the syringe was removed, exposing the composite to

fluid pressure. The tube end was finally inserted into a beaker containing PBS. Sealing time was then assessed with failure determined when dye was visible within the PBS contained within the beaker. Fluid pressure head in the tubes was determined via equation (5):

$$Pressure\,(mmHg) \;=\; p \;x\; g \;x\; h \;x\; 0.007501 \;\; mmHg/Newton \tag{5}$$

where p = the density of DI water, g = gravitational force, and h = tube height, with a final pressure of 146.87 mmHg determined.

4.13 Adhesion Test

Adhesion strength to bone was assessed following a previous method with modifications.[98] Deer bone was cut into rectangular sections approximately 10mm width × 30mm length × 20mm thickness to expose the trabeculae followed by rehydration in PBS for 1 hour. Bone wax or BPLP-Ser composite (~0.5g) was then applied in a uniform layer to one 10mm × 30mm bone face and a second bone face was then adhered to the first using hand pressure for 30s. Attached bone pieces were then incubated in PBS for 24 hours at 37°C under agitation (200rpms). Adhesion strength was tested using a 5966 series advanced electromechanical testing system with a 10kN load cell (Instron, Norwood, MA, USA) and 10kN pneumatic tensile grips. One piece of the adhered bone was first placed within the top tensile grip followed by lowering the crosshead until the other piece was within the bottom grip, taking care not to grip the adhered interface. Tension was then applied at a rate of 1.3mm/min until failure of the adhesive, with peak stress calculated.

Adhesion to native tissue was also assessed qualitatively using chicken drumsticks. First, amputation was simulated via bisection of the femur, exposing the intramedullary cavity. Composite was then packed into the cavity. Additionally, the femoral condyle was separated from the shaft, exposing the interior trabecular faces. BPLP composite was then gently pressed into the exposed face and used to reattach the separated condyle to the main body. Weight bearing capability of the composite was then assessed by lifting the complete drumstick by the reattached condyle.

4.14 Cell culture and medium

Human mesenchymal stem cells (hMSCs, Lonza) were cultured in low glucose Dulbecco's Modified Eagle Medium (DMEM) with 10 vol. % fetal bovine serum (FBS) (Atlanta Biologicals, Flowery Branch, GA), GlutaMAX (Gibco Laboratories, Gaithersburg, MD) and 1% antibiotic antimycotic 100X solution (Invitrogen, Carlsbad, CA). L929 fibroblasts were cultured in DMEM with 10 vol. % FBS and 1% antibiotic antimycotic 100X solution and Eagle's Minimum Essential Medium (MEM) with 10 vol. % FBS 1% antibiotic antimycotic 100X solution.

4.15 Cytotoxicity

To prepare degradation products, 1 g of material was fully degraded in 10 mL 0.2 M NaOH solution followed by adjustment of pH to 7.4 with HCl and NaOH. Solutions were then centrifuged for 10 minutes at 12,000 rpms to fully remove undegraded hydroxyapatite. Degradation products were then sterilized via 0.2μm filter (Agilent, Santa Clara, CA).

Dilutions of degradation products were prepared using culture medium and 10 μL of each dilution were added to L929 cells (with an initial cell density of 3600/well) cultured in 96 well plates with 100 μL medium. After culturing for 24 h, CCK-8 evaluation (Dojindo, Rockville, MD) was performed according to manufacturer's instructions.

4.16 Cell Proliferation

For cell proliferation, degradation product dilutions were prepared using the above procedure. L929 cells with an initial density of 500 cells per well were cultured with chosen dilutions in 96-well plates (10uL per 100uL culture media as above). At designated time points, cell viability was examined by Cell Counting Kit-8 (Dojindo, Rockville, MD) according to manufacturer instructions. Proliferation of hMSCs seeded directly on the surface of BPLP-Ser/50%HA was also studied. hMSCs were seeded at an initial density of 3000 cells/cm^2. At designated time points (Day 1, 3, 7 and 14), cells were lysed with RIPA buffer and DNA was quantified with the Pico Green dsDNA assay (Invitrogen, Carlsbad, CA) according to manufacturer instructions, with proliferation (%) at Days 3, 7, and 14 normalized to Day 1.

4.17 Cell Differentiation Study

hMSCs (<passage 6) were used to study differentiation in the presence of material degradation products. Briefly, cells at ~80% confluence were treated with an established OG medium (low-glucose DMEM with 10−7 M dexamethasone, 0.05 mM ascorbate-2-phosphate, and 0.01 M β-glycerophosphate) supplemented with degradation products (prepared as above) at different concentrations for 14 days with pure OG medium as control.

4.18 ALP assay

For ALP expression analysis, cell samples were lysed using RIPA buffer followed by centrifugation to remove debris. ALP activity was quantified utilizing p-nitrophenyl phosphate (PNPP) (hydrolyzed by ALP into a yellow-colored product). Briefly, PNPP stock solution (1M) was diluted with ALP assay buffer (1:100). 50 μL of diluted buffer was then added to 50 μL of lysate. After 10–30 min of incubation at 37°C, absorbance was measured at 405 nm on a plate reader (infinite M200 PRO, TECAN, Männedorf, Switzerland).

4.19 Alizarin Red staining

For Alizarin Red staining, cell samples were fixed with 4% paraformaldehyde. 40 mM Alizarin red solution was then added to fixed samples followed by 30 minutes of incubation with gentle shaking to stain calcium nodules. After thoroughly washing, the stained cells were observed via Microscope (Nikon, Tokyo, Japan).

4.20 Bacteria Incubation

Staphylococcus aureus (*S. aureus*, ATCC® 6538™) and Escherichia coli (*E. coli*, ATCC® 25922™) were purchased from ATCC (American Type Culture Collection) and used following established safety protocols. Tryptic soy broth (Cat. #: C7141) and tryptic soy agar (Cat. #: C7121) used for *S. aureus* culture were purchased from Criterion (through VWR). Luria broth base (LB broth, Cat. #: 12795–027) and select agar (Cat. #: 30391–

023) used for *E. coli* culture were purchased from Invitrogen. *S. aureus* and *E. coli* were incubated at 37 °C in sterilized tryptic soy broth and LB broth, respectively, with a speed of 150 rpm in a rotary shaker overnight and the obtained bacteria suspensions were diluted to a 0.5 McFarland Standard (optical density (OD) at 600 nm around 0.06 and 0.034 for *S. aureus* and *E coli*, respectively).

4.21 Bacterial Inhibition

The bacterial inhibition of BPLP-Ser/HA putty against both *S. aureus* and *E. coli* was tested via turbidity assay. For each sample, 20mg of ethylene oxide sterilized material was placed in a 96 well plate and immersed in 200 uL of germ containing nutrient solution with a bacterial concentration of 1×10^6 (CFU)/mL (100x dilution from 0.5 McFarland Standard). Incubation was performed at 37 °C on an orbital shaker with a speed of 150 rpm for 24 h. Germ containing growth broth, pure growth broth without bacteria, and commercial bone wax were also tested and served as positive, negative, and material controls, respectively. The bacterial broth medium was then aliquoted, and the OD value of the medium at 600 nm was recorded by a microreader (TECAN, infinite M200 PRO). The inhibition ratios were calculated by equation (6):

$$Inhibition \quad Ratio \quad (\%) = 100 - 100 \quad X \quad \frac{A_t - A_0}{A_{con} - A_0} \tag{6}$$

where A_0 was the OD value of bacterial broth medium before incubation, and A_t and A_{con} were the OD values of material containing medium and germ containing growth medium (control) after incubation, respectively.

4.22 Rat critical sized cranial model

The rat experiments were performed in compliance with a protocol approved by the Institutional Animal Care and Use Committee (IACUC, Approval Number: PRAMS201342878) at the Pennsylvania State University. Sprague-Dawley rats (male, age 8–12 wks, ~200g) were randomly divided into four groups of 6 rats per group for *in vivo* evaluation of BPLP composites. Rats were anesthetized by inhalation of 2–4% isoflurane gas until unresponsive followed by a supplement of ketamine and xylazine anesthesia (80mg/kg and 10mg/kg, respectively). Local anesthesia, buprenorphine, and bupivacaine were then injected subcutaneously at the parietal site. The surgical site was shaved and disinfected by swabbing with 10% povidone iodine solution followed by 70% alcohol and sterile saline swabs. The calvarium was exposed after skin incision (Figure S6a) followed by trephining a circular 8mm diameter cranial bone defect using a low-speed dental drill (Foredom, Bethel, CT) (1500rpm) with saline irrigation to prevent friction based thermal damage to surrounding tissues (Figure S6b–c). The cranial disk was removed and care was taken not to damage the underlying *dura mater* (Figure S6d-e). The site was then flushed with sterile saline solution and the defects were filled with either .25g of BPLP-Ser/50%HA composite or bone wax without applying pressure on the underlying brain (Figure S6f and Figure S7). Autogenous cranial bone was rotated 180 degrees and replaced within the defect to serve as positive control, while defects sans material served as the negative control. The periosteum and skin tissue were closed and sutured with 6–0 VICRYL absorbable sutures.

Rats were euthanized 1 week and 4 weeks post-surgery via carbon dioxide. At each time point, the heads were separated post euthanasia followed by dissection and isolation of the cranial defect for subsequent micro-CT scanning and histology. All animal experiments were carried out in compliance with protocols approved by the Pennsylvania State University Institutional Animal Care and Use Committee.

4.23 uCT analysis

Micro CT imaging was performed using a General Electric v|tome|x L300 nano/microCT (General Electric, Boston, MA) dual-tube system equipped with a 300kV unipolar microfocus X-ray tube, a 180kV nanofocus X-ray tube with transmission target assembly, and a GE DXR250 high-contrast digital flat panel detector. Volumes of interest were selected in Avizo (FEI Company, Hillsboro, OR) from which % bone volume/total volume (BV/TV) was calculated. VOI was defined using an 8mm cylinder (the original defect diameter) with a height greater than the thickness of the defect (~2mm). Thresholding values of new bone were chosen to match the average density value of the native bone by sampling the latter in the region adjacent to but outside the 8mm circular region of interest (ROI) corresponding to the surgically created defect. Threshold values for the BPLP-Ser/50%HA were likewise chosen via an average of the density of the material measured within its bulk.

4.24 Histology

Calvarial bones were fixed in 4% cold paraformaldehyde for 24h at 4°C. Remaining BPLP-Ser/50%HA in the explants was imaged using an in vivo fluorescent imaging system (MaestroTM EX, Woburn, MA) with excitation and emission wavelengths of 370 and 580 nm, respectively. The bone was then decalcified in of 12.5% EDTA and 12.5% 4% paraformaldehyde in 1x phosphate buffered saline (PBS) (pH 7.4) for 8 weeks. Fully decalcified bones were dehydrated in an ascending ethanol series and infiltrated with paraffin wax by a TP1020 tissue processor (Leica, Buffalo Grove, IL). Samples were embedded in wax and 8μm serial slices were sectioned via microtome (Shandon, Charleston, SC). Slices were placed on positively charged microscope slides and dried overnight. The sections were then stained with hematoxylin and eosin using an Autostainer XL (Leica, Buffalo Grove, IL) and observed under light microscopy (Keyence, Woburn, MA).

4.25 Statistical methods

All data was recorded as mean ± standard deviation (SD), unless otherwise stated. Data was analyzed using Microsoft Excel software. For all studies, statistical analysis was performed via one way analysis of variance (ANOVA). Statistical significance was indicated by * $p<0.05$, and sample number n is specifically stated.

Supplementary Material

Refer to Web version on PubMed Central for supplementary material.

Acknowledgements

This work was supported in part by a National Institute of Arthritis and Musculoskeletal and Skin Diseases (NIAMS) award (AR072731).

References

1. Massimo M, Timothy RA, Bone Res. 2013, 1 (3), 203–215. [PubMed: 26273504]
2. Allen-Wilson N, Beatty R, Sharpe J, J Am Podiatr Med Assoc 2015, 105 (1), 74–79. [PubMed: 25675229]
3. Claudio S, Enrico T, Giuseppe B, Vincenzo A, Aldo M, Eur Spine J. 2004, 13, S89–S96. [PubMed: 15221572]
4. Huan Z, Jun G, Yanjie B, Chunyong L, Lei Y, J Orthop Translat. 2019, 17, 64–72. [PubMed: 31194062]
5. Laurel G, Anthony K, Philip W, John EC Jr., Infect Control Hosp Epidemiol. 2004, 25 (4), 346–348. [PubMed: 15108734]
6. Fahradyan A, Ohanisian L, Tsuha M, Park MJ, Hammoudeh JA, J Craniofac Surg 2018, 29 (4), 976–979. [PubMed: 29438209]
7. Tadeusz W, Yuehuei HA, Xuejun W, Qian K, Christopher MH, Jonathan KA, 2008, 466, 481–486.
8. Suwanprateeb J, Suvannapruk W, Thammarakcharoen F, Chokevivat W, Rukskul P, J Mater Sci: Mater Med 2013, 24, 2881–2888. [PubMed: 23955721]
9. Ihsanul A, Heroe S, Puruhito., Asian Cardiovasc Thorac Ann 2020, 29 (3), 203–207. [PubMed: 33353370]
10. Orgill DP, Ehret FW, Regan JF, Glowacki J, Mulliken JB, J Biomed Mater Res. 39 (3), 358–363. [PubMed: 9468043]
11. Wassanai W, Timothy Q, Suthipas P, Solid State Phenom. 2017, 266, 221–225.
12. Weijing C, Shouyang Z, Yin Z, Fan Q, Jun T, Zhenning W, Jiapan L, Mater. Sci. Eng. C 2019, 99, 979–985.
13. Jiaying L, Yang H, Long L, Chao W, Jia W, Yang L, Dafu C, Xiaokang D, Chuanan S, Fujian X, Adv.Sci 2020, 7.
14. Feifei Y, Minchao L, Tie Z, Qi Z, Yan C, Zhibo L, Renxiong W, Lin C, ACS Biomater. Sci. Eng 2021, 7, 663–671. [PubMed: 33502176]
15. Saeid K, Francesco B, Sepideh H, Robert GH, Masoud M, Trends Biotechnol. 2018, 36, 430–444. [PubMed: 29397989]
16. Xie D; Guo J; Mehdizadeh M; Tran RT; Chen R; Sun D; Qian G; Jin D; Bai X; Yang J, J Mater Chem B 2015, 3, 387–398. DOI 10.1039/C4TB01498G. [PubMed: 25580247]
17. Bai S; Zhang X; Lv X; Zhang M; Huang X; Shi Y; Lu C; Song J; Yang H, Advanced Functional Materials 2020, 30 (5), 1908381.
18. Tarafder S; Park GY; Felix J; Lee CH, Acta Biomater 2020, 117, 77–92. DOI 10.1016/j.actbio.2020.09.050. [PubMed: 33031966]
19. Yang J; Webb AR; Ameer GA, Advanced Materials 2004, 16 (6), 511–516.
20. Motlagh D; Allen J; Hoshi R; Yang J; Lui K; Ameer G, Journal of Biomedical Materials Research Part A: An Official Journal of The Society for Biomaterials, The Japanese Society for Biomaterials, and The Australian Society for Biomaterials and the Korean Society for Biomaterials 2007, 82 (4), 907–916.
21. Su L-C; Xie Z; Zhang Y; Nguyen KT; Yang J, Frontiers in Bioengineering and Biotechnology 2014, 2 (23). DOI 10.3389/fbioe.2014.00023.
22. Guo J; Xie Z; Tran RT; Xie D; Jin D; Bai X; Yang J, Advanced materials 2014, 26 (12), 1906–1911. [PubMed: 24375469]
23. Dey J; Xu H; Nguyen KT; Yang J, J Biomed Mater Res A 2010, 95 (2), 361–70. DOI 10.1002/jbm.a.32846. [PubMed: 20629026]
24. Sun DW; Chen YH; Tran RT; Xu S; Xie DH; Jia CH; Wang YC; Guo Y; Zhang ZM; Guo JS; Yang J; Jin D; Bai XC, Sci Rep-Uk 2014, 4. DOI ARTN6912 10.1038/srep06912.
25. Guo JS; Xie ZW; Tran RT; Xie DH; Jin DD; Bai XC; Yang J, Adv Mater 2014, 26 (12), 1906–1911. DOI 10.1002/adma.201305162. [PubMed: 24375469]
26. Dey J; Tran RT; Shen J; Tang L; Yang J, Macromol Mater Eng 2011, 296 (12), 1149–1157. DOI 10.1002/mame.201100074. [PubMed: 22184499]

27. Gyawali D; Nair P; Zhang Y; Tran RT; Zhang C; Samchukov M; Makarov M; Kim HKW; Yang JA, Biomaterials 2010, 31 (34), 9092–9105. DOI 10.1016/j.biomaterials.2010.08.022. [PubMed: 20800893]
28. Tran RT; Thevenot P; Gyawali D; Chiao JC; Tang L; Yang J, Soft Matter 2010, 6 (11), 2449–2461. DOI 10.1039/C001605E. [PubMed: 22162975]
29. Jiao Y; Gyawali D; Stark JM; Akcora P; Nair P; Tran RT; Yang J, Soft Matter 2012, 8 (5), 1499–1507. DOI 10.1039/c1sm05786c. [PubMed: 25309615]
30. Tran RT; Palmer M; Tang SJ; Abell TL; Yang J, Gastrointest Endosc 2012, 75 (5), 1092–1097. DOI 10.1016/j.gie.2011.12.009. [PubMed: 22301346]
31. Yang J; Zhang Y; Gautam S; Liu L; Dey J; Chen W; Mason RP; Serrano CA; Schug KA; Tang L, Proc Natl Acad Sci U S A 2009, 106 (25), 10086–91. DOI 10.1073/pnas.0900004106. [PubMed: 19506254]
32. Xie ZW; Zhang Y; Liu L; Weng H; Mason RP; Tang LP; Nguyen KT; Hsieh JT; Yang J, Adv Mater 2014, 26 (26), 4491-+. DOI 10.1002/adma.201306070. [PubMed: 24668888]
33. Zhang Y; Tran RT; Qattan IS; Tsai YT; Tang LP; Liu C; Yang J, Biomaterials 2013, 34 (16), 4048–4056. DOI 10.1016/j.biomaterials.2013.02.040. [PubMed: 23465824]
34. Hu JQ; Guo JS; Xie ZW; Shan DY; Gerhard E; Qian GY; Yang J, Acta Biomater 2016, 29, 307–319. DOI 10.1016/j.actbio.2015.10.010. [PubMed: 26463014]
35. Mehdizadeh M; Weng H; Gyawali D; Tang L; Yang J, Biomaterials 2012, 33 (32), 7972–83. DOI 10.1016/j.biomaterials.2012.07.055. [PubMed: 22902057]
36. Guo J; Kim GB; Shan D; Kim JP; Hu J; Wang W; Hamad FG; Qian G; Rizk EB; Yang J, Biomaterials 2017, 112, 275–286. DOI 10.1016/j.biomaterials.2016.10.010. [PubMed: 27770631]
37. Su LC; Xie Z; Zhang Y; Nguyen KT; Yang J, Front Bioeng Biotechnol 2014, 2, 23. DOI 10.3389/fbioe.2014.00023. [PubMed: 25023605]
38. Hongjin Q, Jian Y, Pradeep K, Jason K, Guillermo AA, Biomaterials. 2006, 27, 5845–5854. [PubMed: 16919720]
39. Jian Y, Yi Z, Santosh G, Li L, Jagannath D, Wei C, Ralph PM, Carlos AS, Kevin AS, and Liping T, PNAS 2009, 106, 10086–10091. [PubMed: 19506254]
40. Kim JP; Xie ZW; Creer M; Liu ZW; Yang J, Chem Sci 2017, 8 (1), 550–558. DOI 10.1039/c6sc02962k. [PubMed: 28348728]
41. Ma C; Tian X; Kim JP; Xie D; Ao X; Shan D; Lin Q; Hudock MR; Bai X; Yang J, Proc Natl Acad Sci U S A 2018, 115 (50), E11741–E11750. DOI 10.1073/pnas.1813000115. [PubMed: 30478052]
42. Ma CY; Kuzma ML; Bai XOC; Yang J, Adv Sci 2019, 6 (19). DOI ARTN 1900819 10.1002/advs.201900819.
43. Al-Sharifi E; Alkaisy N; Al-Mahmood A, Biomedical Research-tokyo 2019, 30, 406–409.
44. Cui Y; Zhu T; Li A; Liu B; Cui Z; Qiao Y; Tian Y; Qiu D, ACS applied materials & interfaces 2018, 10 (8), 6956–6964. [PubMed: 29411600]
45. Zheng X; Liu Y; Liu Y; Pan Y; Yao Q, Journal of Biomedical Materials Research Part B: Applied Biomaterials 2021, 109 (4), 517–526. [PubMed: 32864862]
46. Soundarya SP; Menon AH; Chandran SV; Selvamurugan N, International journal of biological macromolecules 2018, 119, 1228–1239. [PubMed: 30107161]
47. Zhang D; Wu X; Chen J; Lin K, The development of collagen based composite scaffolds for bone regeneration. Bioact Mater 3: 129–138. 2018. [PubMed: 29744450]
48. Alizadeh-Osgouei M; Li Y; Wen C, Bioactive materials 2019, 4, 22–36. [PubMed: 30533554]
49. Koons GL; Diba M; Mikos AG, Nature Reviews Materials 2020, 5 (8), 584–603.
50. Sun D; Chen Y; Tran RT; Xu S; Xie D; Jia C; Wang Y; Guo Y; Zhang Z; Guo J, Scientific reports 2014, 4 (1), 1–9.
51. Tang J; Guo J; Li Z; Yang C; Xie D; Chen J; Li S; Li S; Kim GB; Bai X, Journal of Materials Chemistry B 2015, 3 (27), 5569–5576. [PubMed: 26213625]
52. Xie D; Guo J; Mehdizadeh MR; Tran RT; Chen R; Sun D; Qian G; Jin D; Bai X; Yang J, Journal of Materials Chemistry B 2015, 3 (3), 387–398. [PubMed: 25580247]
53. Guo J; Tian X; Xie D; Rahn K; Gerhard E; Kuzma ML; Zhou D; Dong C; Bai X; Lu Z, Advanced Functional Materials 2020, 30 (27), 2002438.

54. Qiu X; Chen L; Hu J; Sun J; Hong Z; Liu A; Chen X; Jing X, Journal of Polymer Science Part A: Polymer Chemistry 2005, 43 (21), 5177–5185.
55. Xie R; Hu J; Ng F; Tan L; Qin T; Zhang M; Guo X, Ceramics International 2017, 43 (6), 4794–4802.
56. Wang Z; Chen L; Wang Y; Chen X; Zhang P, ACS applied materials & interfaces 2016, 8 (40), 26559–26569. [PubMed: 27649958]
57. Nabipour H; Batool S; Hu Y, Emergent Materials 2021, 1–14.
58. Jiang W; Griffanti G; Tamimi F; McKee MD; Nazhat SN, Journal of Structural Biology 2020, 212 (1), 107592. [PubMed: 32736073]
59. Shao C; Zhao R; Jiang S; Yao S; Wu Z; Jin B; Yang Y; Pan H; Tang R, Advanced Materials 2018, 30 (8), 1704876.
60. Ruiz-Agudo E; Ruiz-Agudo C; Di Lorenzo F; Alvarez-Lloret P; Ibañez-Velasco A; Rodriguez-Navarro C, ACS Biomaterials Science & Engineering 2021.
61. Davies E; Müller KH; Wong WC; Pickard CJ; Reid DG; Skepper JN; Duer MJ, Proceedings of the National Academy of Sciences 2014, 111 (14), E1354–E1363.
62. Hu Y-Y; Rawal A; Schmidt-Rohr K, Proceedings of the national academy of sciences 2010, 107 (52), 22425–22429.
63. Zeng J; Yang S; Yu H; Xu Z; Quan X; Zhou J, Langmuir 2021, 37 (11), 3410–3419. [PubMed: 33691409]
64. Xie Z; Kim JP; Cai Q; Zhang Y; Guo J; Dhami RS; Li L; Kong B; Su Y; Schug KA; Yang J, Acta Biomater 2017, 50, 361–369. DOI 10.1016/j.actbio.2017.01.019. [PubMed: 28069502]
65. Tran RT; Wang L; Zhang C; Huang M; Tang W; Zhang C; Zhang Z; Jin D; Banik B; Brown JL, Journal of Biomedical Materials Research Part A 2014, 102 (8), 2521–2532. [PubMed: 23996976]
66. Burr DB; Allen MR, Basic and applied bone biology. Academic Press: 2019.
67. Willie BM; Petersen A; Schmidt-Bleek K; Cipitria A; Mehta M; Strube P; Lienau J; Wildemann B; Fratzl P; Duda G, Soft Matter 2010, 6 (20), 4976–4987.
68. Zhang B; DeBartolo JE; Song J, ACS applied materials & interfaces 2017, 9 (5), 4450–4456. [PubMed: 28125208]
69. Serrano MC; Carbajal L; Ameer GA, Advanced Materials 2011, 23 (19), 2211–2215. [PubMed: 21557337]
70. Zaky S; Lee K; Gao J; Jensen A; Verdelis K; Wang Y; Almarza A; Sfeir C, Acta biomaterialia 2017, 54, 95–106. [PubMed: 28110067]
71. Lv H; Wang H; Zhang Z; Yang W; Liu W; Li Y; Li L, Life sciences 2017, 178, 42–48. [PubMed: 28433510]
72. Shan D; Kothapalli SR; Ravnic DJ; Gerhard E; Kim JP; Guo J; Ma C; Guo J; Gui L; Sun L, Advanced functional materials 2018, 28 (34), 1801787. [PubMed: 31588204]
73. Pfeilschifter J; Mundy GR, Proceedings of the National Academy of Sciences 1987, 84 (7), 2024–2028.
74. Lu X; Shi S; Li H; Gerhard E; Lu Z; Tan X; Li W; Rahn KM; Xie D; Xu G, Biomaterials 2020, 232, 119719. [PubMed: 31901688]
75. Peterson J; Dechow PC, The Anatomical Record Part A: Discoveries in Molecular, Cellular, and Evolutionary Biology: An Official Publication of the American Association of Anatomists 2003, 274 (1), 785–797.
76. Nooh N; Abdullah WA; Grawish ME-A; Ramalingam S; Javed F; Al-Hezaimi K, Indian journal of orthopaedics 2014, 48 (3), 319–325. [PubMed: 24932041]
77. Suwanprateeb J; Suvannapruk W; Thammarakcharoen F; Chokevivat W; Rukskul P, Journal of Materials Science: Materials in Medicine 2013, 24 (12), 2881–2888. [PubMed: 23955721]
78. Golubeva OY; Ulyanova NY; Vladimirova EV; Shamova OV, Langmuir 2021, 37 (42), 12356–12364. [PubMed: 34643405]
79. Ivanov I, Biochimica et Biophysica Acta (BBA)-Biomembranes 1999, 1415 (2), 349–360. [PubMed: 9889396]
80. Avery RK; Albadawi H; Akbari M; Zhang YS; Duggan MJ; Sahani DV; Olsen BD; Khademhosseini A; Oklu R, Science translational medicine 2016, 8 (365), 365ra156–365ra156.

81. Gaharwar AK; Avery RK; Assmann A; Paul A; McKinley GH; Khademhosseini A; Olsen BD, ACS nano 2014, 8 (10), 9833–9842. [PubMed: 25221894]
82. Kumar VA; Taylor NL; Jalan AA; Hwang LK; Wang BK; Hartgerink JD, Biomacromolecules 2014, 15 (4), 1484–1490. [PubMed: 24694012]
83. Brückner T; Schamel M; Kübler AC; Groll J; Gbureck U, Acta biomaterialia 2016, 33, 252–263. [PubMed: 26805427]
84. Macfarlane R, Journal of clinical pathology 1948, 1 (3), 113. [PubMed: 16810794]
85. Hofman AH; van Hees IA; Yang J; Kamperman M, Adv Mater 2018, 30 (19), e1704640. DOI 10.1002/adma.201704640. [PubMed: 29356146]
86. Xiong Y; Zhang X; Ma X; Wang W; Yan F; Zhao X; Chu X; Xu W; Sun C, Polymer Chemistry 2021.
87. Duan S; Wu R; Xiong Y-H; Ren H-M; Lei C; Zhao Y-Q; Zhang X-Y; Xu F-J, Progress in Materials Science 2021, 100887.
88. Mittapally S; Taranum R; Parveen S, Journal of Drug Delivery and Therapeutics 2018, 8 (6-s), 411–419.
89. Guo J; Wang W; Hu J; Xie D; Gerhard E; Nisic M; Shan D; Qian G; Zheng S; Yang J, Biomaterials 2016, 85, 204–217. [PubMed: 26874283]
90. Ma C; Gerhard E; Lu D; Yang J, Biomaterials 2018, 178, 383–400. [PubMed: 29759730]
91. Ma C; Gerhard E; Lin Q; Xia S; Armstrong AD; Yang J, Bioactive materials 2018, 3 (1), 19–27. [PubMed: 29744439]
92. Thalji G; Gretzer C; Cooper LF, Bone 2013, 52 (1), 444–453. [PubMed: 22884725]
93. Granchi D; Torreggiani E; Massa A; Caudarella R; Di Pompo G; Baldini N, PloS one 2017, 12 (7), e0181230. [PubMed: 28715463]
94. He Y; Li QY; Ma CY; Xie DH; Li LM; Zhao YT; Shan DY; Chomos SK; Dong C; Tierney JW; Sun L; Lu D; Gui L; Yang J, Acta Biomater 2019, 93, 180–191. DOI 10.1016/j.actbio.2019.03.050. [PubMed: 30926580]
95. Dupoirieux L; Pourquier D; Picot M; Neves M, International journal of oral and maxillofacial surgery 2001, 30 (1), 58–62. [PubMed: 11289623]
96. Spicer PP; Kretlow JD; Young S; Jansen JA; Kasper FK; Mikos AG, Nature protocols 2012, 7 (10), 1918–1929. [PubMed: 23018195]
97. Albadawi H; Altun I; Hu J; Zhang Z; Panda A; Kim HJ; Khademhosseini A; Oklu R, Advanced Science 2021, 8 (1), 2003327.
98. Bou-Francis A; Ghanem A, International Journal of Adhesion and Adhesives 2017, 77, 96–101.

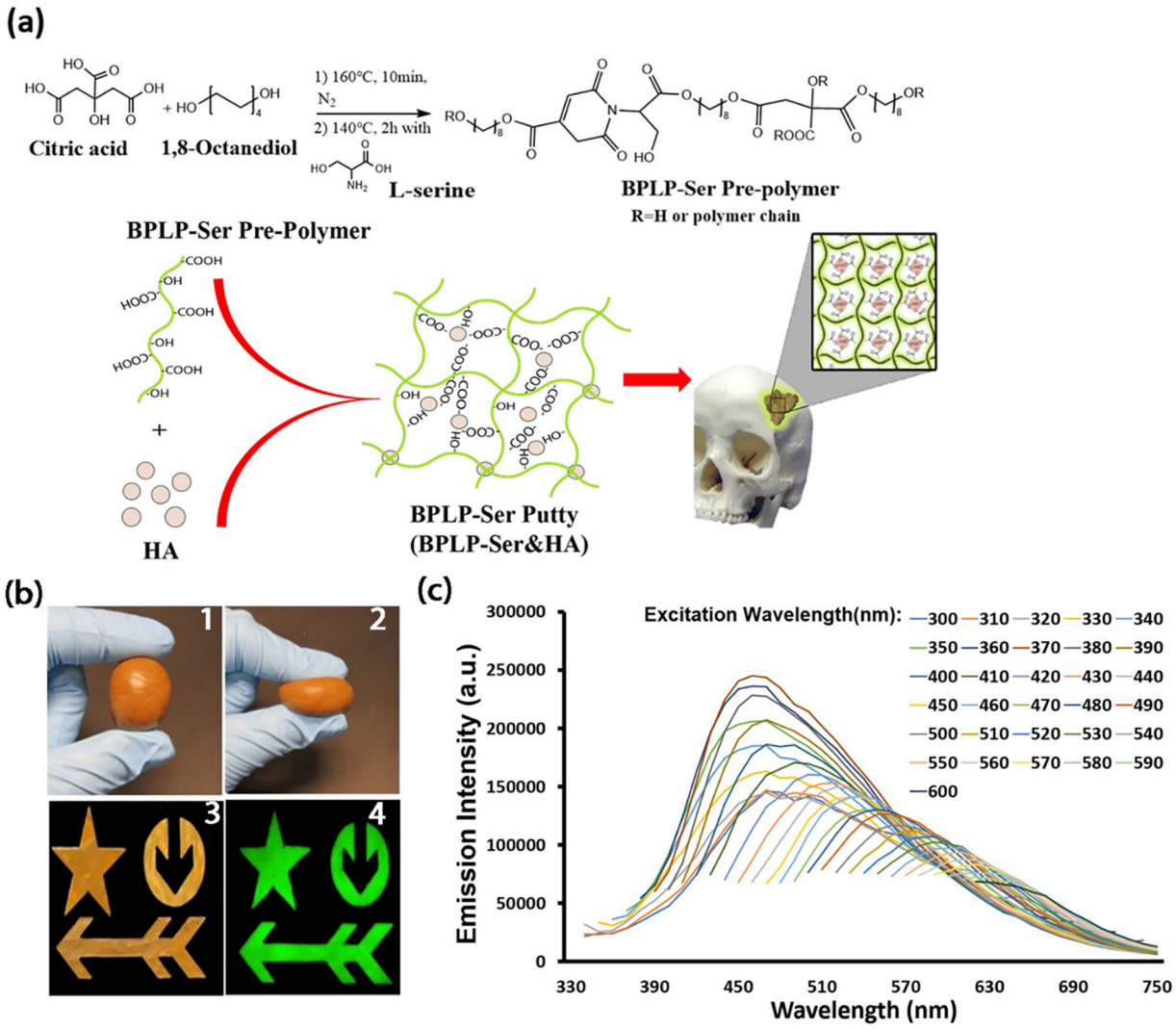

Figure 1: Design of multi-functional BPLP-Ser/HA bone putty.

(a) Schematic demonstration showing the synthesis of BPLP-Ser, fabrication of citrate-based fluorescent composites (BPLP-Ser/HA), and press-fit into irregular cranial defects. (b) BPLP-Ser/65%HA putty (1) is highly malleable and can be molded in different shapes (2 and 3) while displaying excellent fluorescent emission (580nm) (4). (c) Emission spectra of BPLP-Ser/50%HA putty under excitation from 330–600m, demonstrating excitation dependent fluorescent emission.

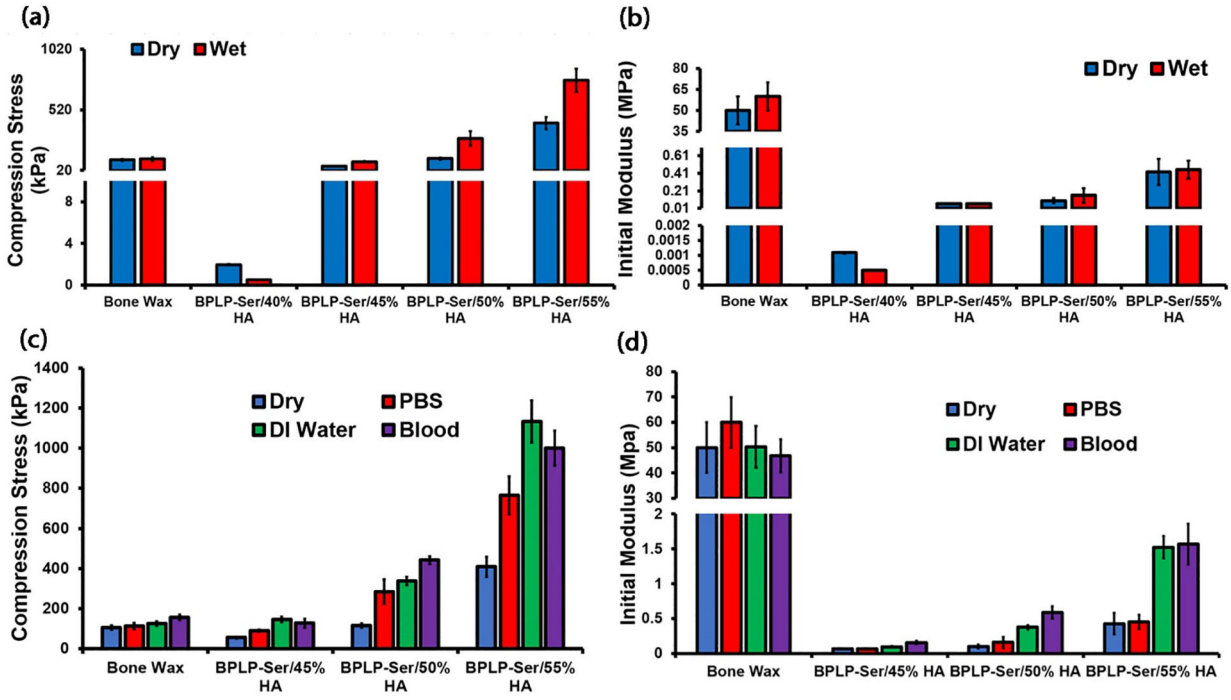

Figure 2: Mechanical properties of commercial Bone Wax and BPLP-Ser/HA putty.

(a) Peak stress and (b) Initial modulus of Bone Wax and BPLP-Ser putty with 40%, 45%, 50%, and 55% HA when compressed to 50% strain in dry and wet (24hrs in 1x PBS) conditions. (c) Peak stress and (d) Initial modulus of the wet-conditioned (24hrs in 1x PBS, DI water, or bovine whole blood) Bone Wax and BPLP-Ser putty with 45%, 50%, and 55% HA when compressed to 50% strain, n ≥5.

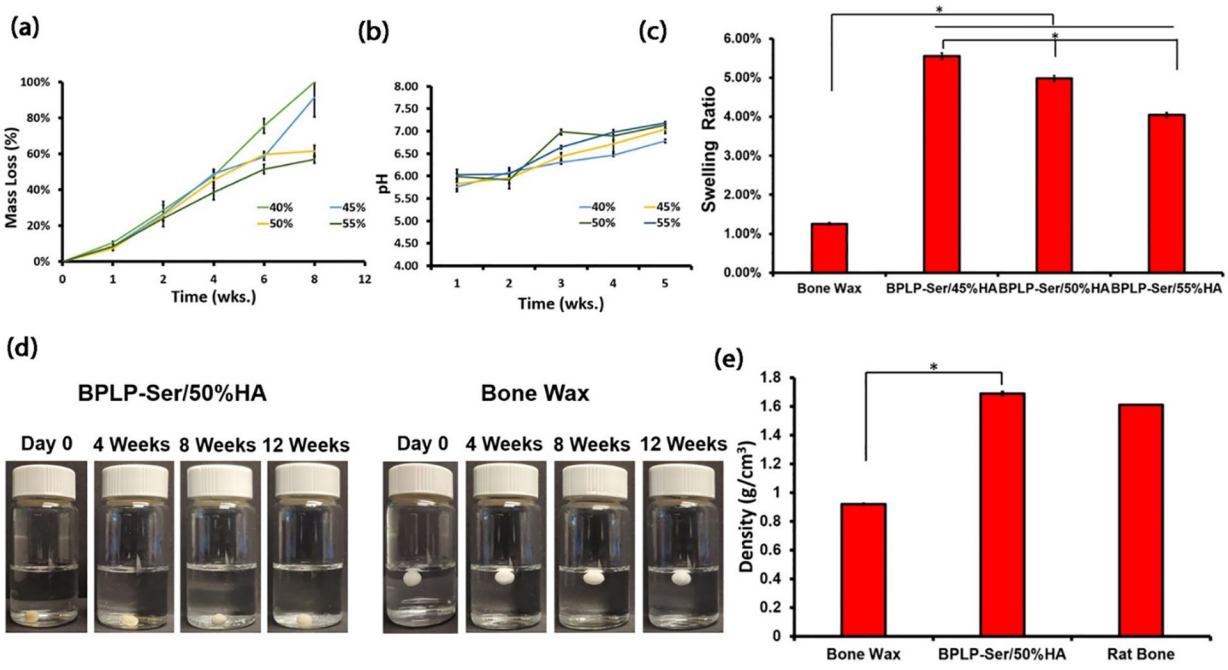

Figure 3: Physical characterization of BPLP-Ser/HA putty.

(a) Mass loss of BPLP-Ser/HA putty over 8 weeks. (b) pH evolution of BPLP-Ser/HA putty degradation media within 5 weeks. (c) swelling ratios of bone wax and BPLP-Ser/HA putty after 24h immerion in 1xPBS (d) Stability of Bone Wax and BPLP-Ser/50%HA in 1x PBS over 12 weeks. (e) Density of Bone Wax, BPLP-Ser/50%HA putty and rat calverial bone. * p<0.05, n ≥6 except for (c) (n ≥3).

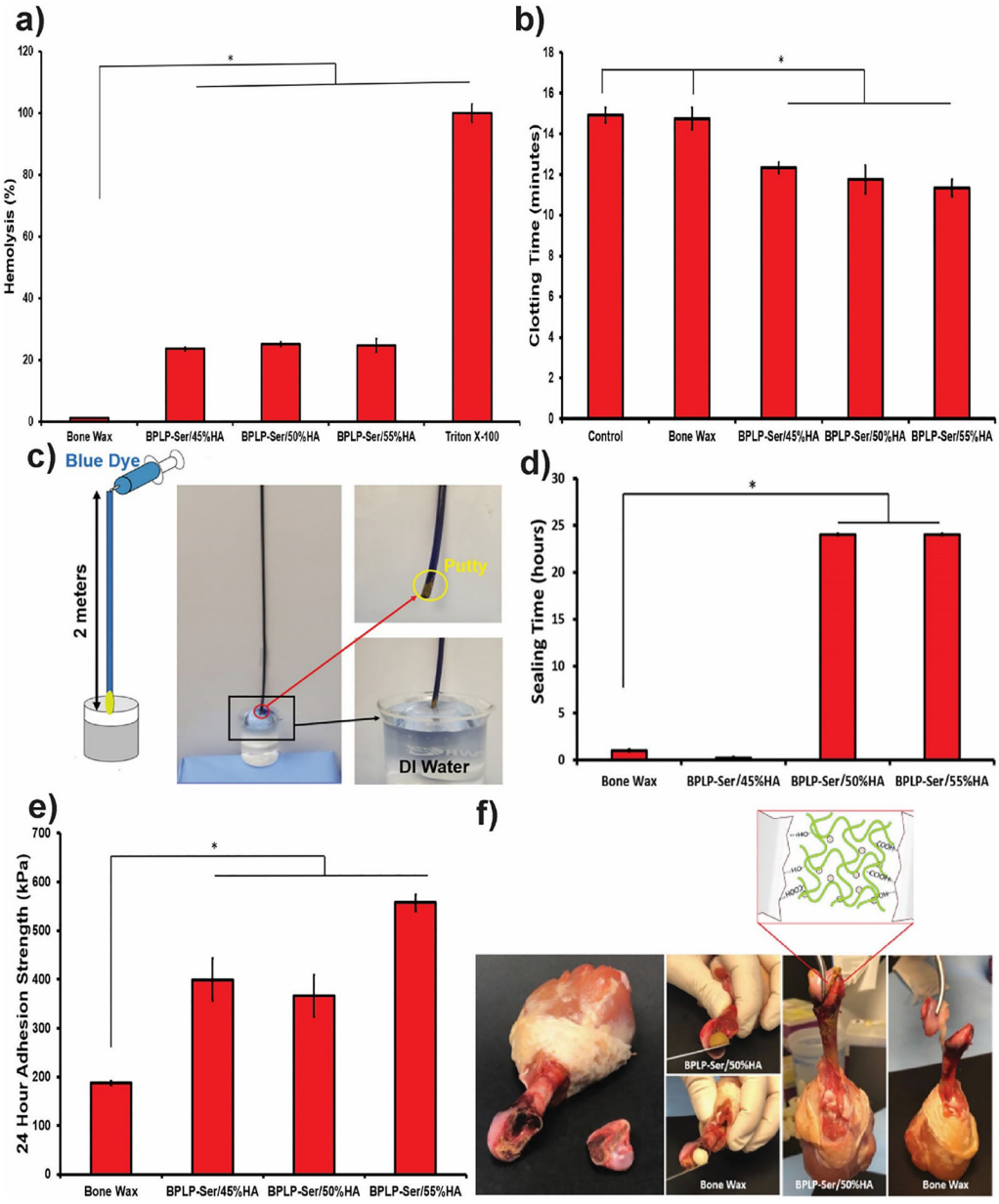

Figure 4: Liquid sealing and adhesion tests of BPLP-Ser/HA putty.

(a) Hemolytic properties of Bone Wax and BPLP-Ser/HA putty. (b) Whole blood clotting time of Bone Wax and BPLP-Ser/HA putty. (c) Schematic demonstration and photographs of sealing experiments at 37°C; a two-meter tube was placed vertically against the wall, then blue dye was injected through the upper end of the tube to simulate physiological blood pressure. The lower end of the tube was plugged with Bone Wax or BPLP-Ser/HA putty after which the lower tube end was immersed in DI water, wetting the materials from the outside. (d) Liquid sealing time of Bone Wax and BPLP-Ser/HA putty at 37°C. (e) Adhesion strength of Bone Wax and BPLP-Ser/HA putty to trabecular bone after 24 hours in PBS. (f) In vitro adhesion of separated femoral condyle and femur via Bone Wax and

BPLP-Ser/50%HA putty and illustration of proposed mechanism for the adhesive property of BPLP-Ser/HA putty. * $p<0.05$, n ≥3.

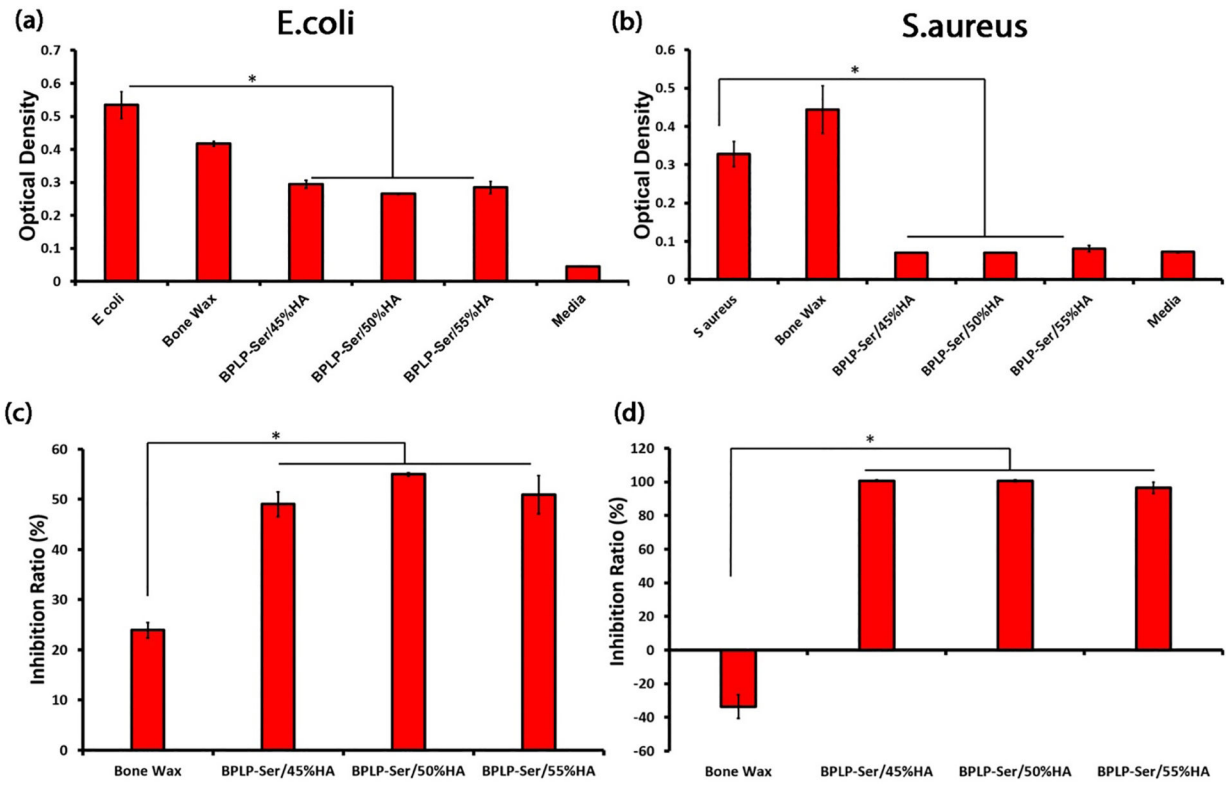

Figure 5: In vitro antibacterial effects of BPLP-Ser/HA putty.

Optical density of *E.coli* (a) and *S.aureus* (b) incubation broth with and without the addition of Bone Wax and BPLP-Ser/HA putties. Inhibition ratios against *E.coli* (c) and *S.aureus* (d) of Bone Wax and BPLP-Ser/HA putty for 24h. * $p<0.05$, n ≥4.

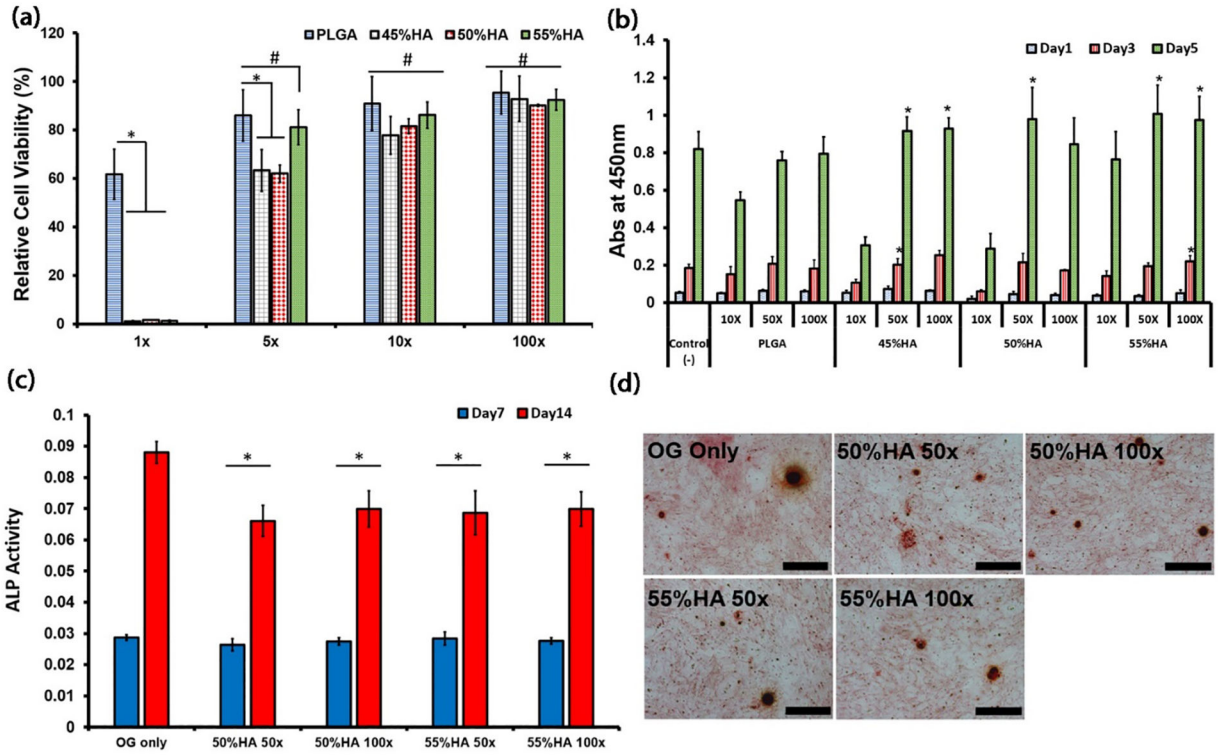

Figure 6: In vitro cytotoxicity, proliferation, and osteogenic capability of BPLP-Ser/HA putty.

(a) 24hr cytotoxicity of degradation products of PLGA and BPLP-Ser/HA putty at 1x, 5x, 10x, and 100x dilution factors against L929 cells. (b) Cell proliferation of L929 cells in the presence of degradation products at 10x, 50x, and 100x dilution factors. (c) ALP production of human mesenchymal stem cells (hMSCs) cultured in OG medium and OG medium containing degradation products of BPLP-Ser/HA putty at 50x and 100x dilution factors. (d) Calcium deposition of hMSCs cultured in OG medium and BPLP-Ser/50%HA and OG medium containing BPLP-Ser/55%HA degradation products at 50x and 100x dilution factors, scale bar=500μm. * $p<0.05$, # $p>0.05$, n≥3.

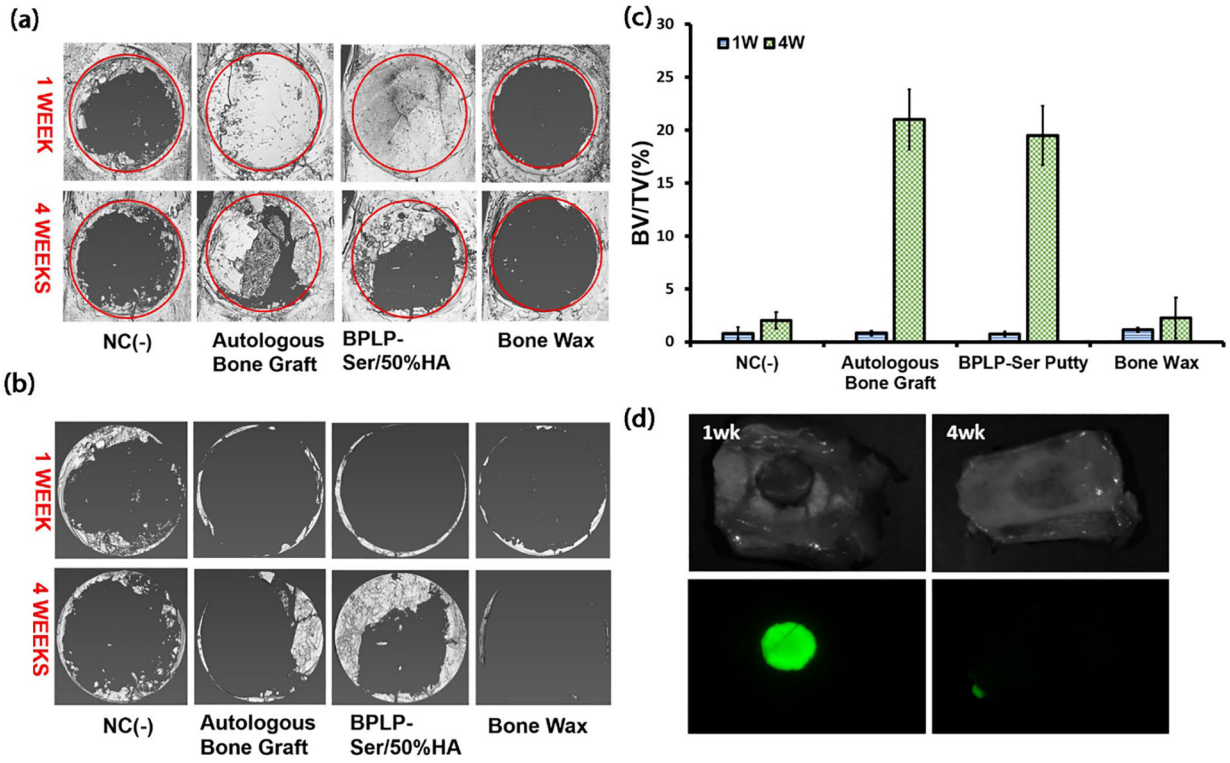

Figure 7: In vivo efficacy of BPLP-Ser/50%HA putty in critical size cranial defects.

(a) Representative micro-computed tomography (μCT) scans 1 week and 4 weeks post-surgery (red circles indicate original 8mm defect diameter). (b) μCT scans of regenerated cranial bone at 1 week and 4 weeks with remaining BPLP-Ser/50%HA and autograft removed to highlight new bone growth. (c) Ratio of new bone volume to total volume at 1 week and 4 weeks (d) Remaining fluorescent signal of explanted materials at 1 and 4 weeks post-surgery. NC(−) = negative control. n=3.

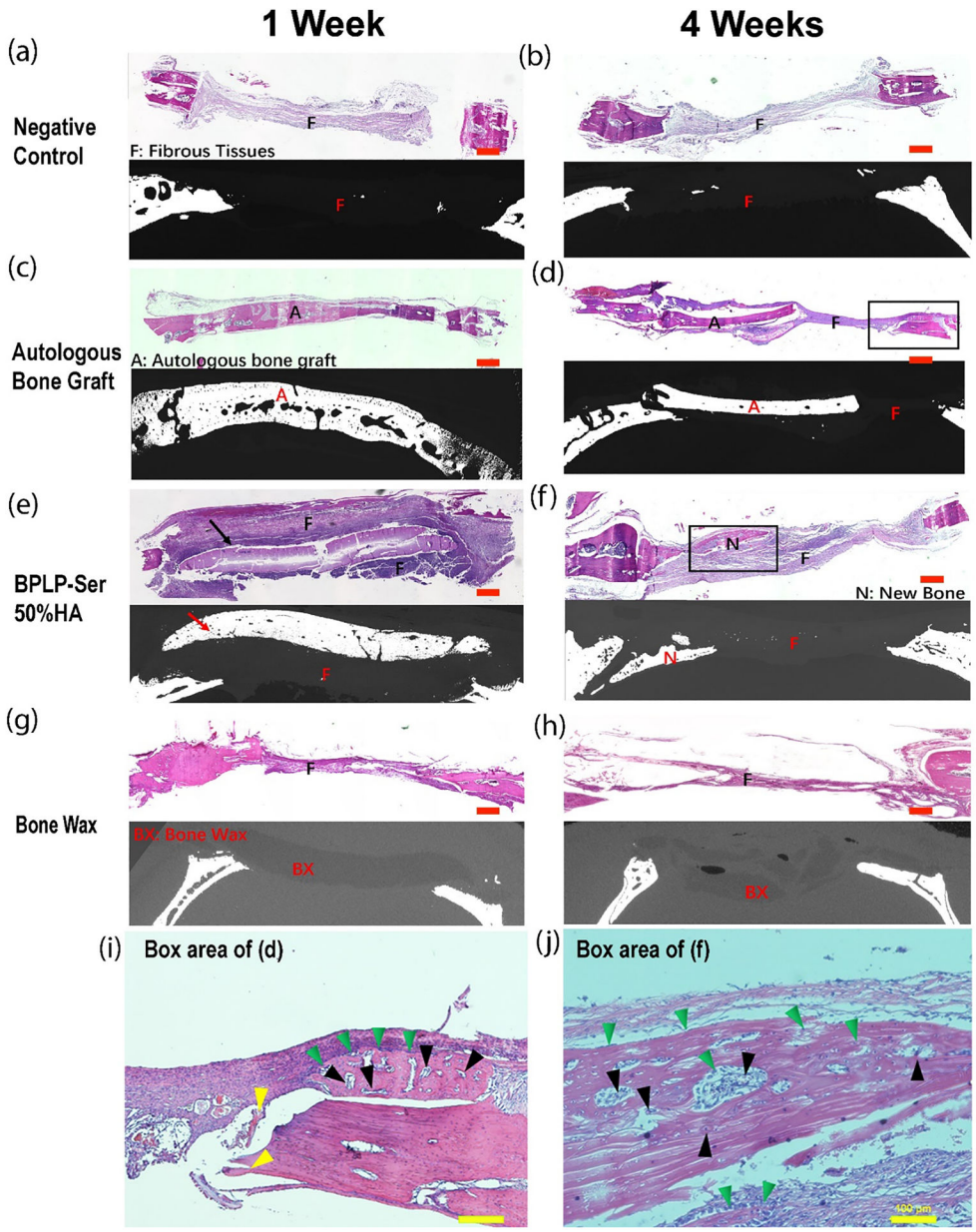

Figure 8: Histological results of cranial defect repair.

Representative H&E-stained tissue sections and corresponding micro-computed tomography (μCT) scans at 1 week and 4 weeks. (a-b) negative control (NC(−)), (c-d) autologous bone graft, (e-f) BPLP-Ser/50%HA putty, and (g-h) bone wax 1 week (a,c,e, and g) and 4 weeks (b,d,f, and h) postoperatively. Scale bar = 300 nm. Arrows indicate BPLP-Ser/50%HA putty. (i-j) Higher magnification images of the boxed region of (d) and (f), respectively. Scale bar=100μm. “F” indicates fibrous repair tissue, “A” represents the autologous bone graft, “N” denotes new bone formation, and “BX” represents bone wax. In images (i and j), green triangles indicate osteoblasts, black triangles represent blood vessels, and yellow triangles mark residual autologous bone.